Efficient Polarisation Measurement for Quantum Cryptography

Soh Kee Pang

An academic exercise presented in partial fulfilment for the degree of Bachelor of Science with Honours in Physics.

Supervisors: Associate Professor Christian Kurfsiefer and
Assistant Professor Antia Lamas-Linares

Department of Physics
National University of Singapore

2005/2006

Acknowledgements

This project, which spanned more than half a year, would not have been possible without the help and support of a few people.

Heartfelt thanks to my supervisors Prof Christian and Prof Antia, for giving me this opportunity to work on this project, and for their advice and support throughout this period.

Special thanks to Alexander Ling, my lab partner, for the helpful discussions, and for his patience and kindness in answering the many questions I have. It has been a pleasure working with him.

And not forgetting all the great people working in the laboratory, who always manage to liven up the atmosphere with their humour. I thank them for always kindly tolerating my presence as I linger around in the laboratory and fiddle with the equipments.

Kee Pang

30 March 2006

To all who seek to better understand this world in which we live in.

Abstract

Quantum state measurements on polarised photonic qubits are performed using an optimal polarimeter. The detailed procedure for building this four-detector polarimeter is presented. The methods for reconstructing the polarisation states of single-photon ensembles and the probability density matrix of correlated photon-pairs are then discussed. Using a coherent light beam (laser) as our single-photon ensembles, the Stokes vectors of the prepared polarisation states are compared with those reconstructed from the measurements, and a fidelity of at least 99.4±0.5 % is observed. A down-converted light source is used to generate the Bell states, which are entangled two-qubit states, and the density matrices constructed for the different states give a minimum fidelity of 96.7±0.3 %. Such a polarimeter will be useful in the field of quantum information. In particular, a recently proposed scheme for key distribution requires the use of an optimal polarimeter presented in this work.

Contents

Appendix

Introduction

Quantum state tomography is the process by which an identical ensemble of unknown quantum states is completely characterised. By itself, quantum state characterisation has a fundamental interest of its own, since it concerns the quantum description of physical systems. The recent years, however, have seen this subject become an area of intensive research and investigation due to the emerging discipline of quantum information.

To characterise quantum states, one naturally has to first create and manipulate them. Their manipulation allows information to be encoded, and hence the term quantum bits – or qubits for short – is coined. Experimental representations of qubit systems include systems of spin-½ particles, two-level atoms, as well as polarisation of photons.

The polarisation of photons, in particular, is attractive because of the ease with which it can be easily manipulated by conventional optical devices. Characterising the polarisation of light requires one to first measure it – a science known as polarimetry. This jargon, of course, comes from classical optics. Ever since George Stokes first conceived of four parameters to completely represent the polarisation of light in 1852, the insights gained from the last 150 years of progress in classical optics have proven to be invaluable in the present efforts to characterise polarised photonic states.

This project involves adopting and applying the classical techniques of polarimetry to experimental measurements of photonic quantum states.

A four-detector polarimeter is built to perform characterisation of polarised photonic qubits. This is based on a minimal tomography method that is recently proposed by Řeháček *et al.* [1]. For the simplest case of single-qubit system, we use a coherent light beam as our single-photon source and estimate its polarisation states. The down-converted light source is then used to generate Bell states, which are entangled two-qubit states, and the density matrix constructed for the system. Our experiment differs from the one carried out by James *et al.* [2] in that our polarimeter is an efficient one – efficient in the sense that it is minimal (no redundancy in the information collected) and optimal (having the least errors).

A polarimeter like the one we have will be useful in the field of quantum cryptography. In particular, a recently proposed protocol for quantum key distribution [3, 4] makes use of minimal state tomography to achieve a higher efficiency than existing protocols.

We begin with a visit to the domain of classical optics and review some of the important concepts on polarisation of light in chapter 1. These concepts will serve as useful tools when we give an introduction to quantum states tomography for single- and pair- photonic qubits in chapter 2. Following that, in chapter 3, we explain the general strategy behind optimising polarimeters, after which we proceed to describe in detail the construction of our polarimeter in chapter 4. Results and analysis of our tomographic measurements are shown in chapter 5. Finally, in chapter 6, we close with a summary.

CHAPTER 1

Polarisation of Light Waves

1.1. The concept of polarisation

Polarisation is a property common to all vector waves. It refers to the temporal behaviour of one of the field vectors appropriate to that wave, observed at a fixed point in space. For light waves, which are transverse electromagnetic waves, the electric field strength $\boldsymbol{E}$ is chosen to define the state of polarisation. In this chapter, we present some mathematical constructs for describing polarisation of light. The treatment of this subject follows closely to that given in Hecht's *Optics* [5].

1.1.1. Stokes Parameters and Stokes Vector

The polarisation of light can be characterized by the Stokes vector, first conceived in 1852 by G. G. Stokes. It consists of four quantities which are functions only of observables of the electromagnetic wave. In other words, these quantities can be measured and obtain directly from experiment. This can be done with a set of four filters, each having a transmittance of 0.5 for incident, unpolarised light.

The first filter will have to be isotropic, passing all polarisation states equally. The second filter is opaque to vertically polarised light; the third filter to -45^{o} polarised light; and the fourth to left-circularly polarised light. If each of these filters is placed alone in the path of the beam under investigation, and the corresponding transmitted irradiances I_0, I_1, I_2, I_3 are measured using a polarisation independent detector, then the four Stokes parameters can be computed by the following relations:

$$S_0 = 2I_0 \,, \tag{1.1a}$$

$$S_1 = 2I_1 - 2I_0 \,, \tag{1.1b}$$

$$S_2 = 2I_2 - 2I_0 \,, \tag{1.1c}$$

$$S_3 = 2I_3 - 2I_0 \,. \tag{1.1d}$$

We can see from the above relations that S_0 is simply the incident irradiance. S_1 is the tendency of the light to be horizontally polarised. S_2 and S_3 are the tendency of the light to be +45^o and right-circularly polarised respectively. The parameter S_1 will be positive when light exhibit a preference for horizontal polarisation, negative if the preference is for vertical polarisation, zero if there is no preference between these two states. Similar arguments hold for S_2 and S_3. Only three of these four parameters will be independent for completely polarised light, since they will then obey the identity:

$$S_0^2 = S_1^2 + S_2^2 + S_3^2 \,. \tag{1.2}$$

Having understood the significance of each of the Stokes parameters, it is more useful for us to cast eq. (1.1) into another form[1]. Letting I_H, I_V, I_{+45}, I_{-45}, I_R and I_L, represent the transmitted intensities of horizontally, vertically, +45^o, –45^o, right- and left-circularly polarised light, we have

$$S_0 \;=\; I_H + I_V \;=\; I_{+45} + I_{-45} \;=\; I_R + I_L \;\;, \tag{1.3a}$$

$$S_1 \;=\; I_H - I_V \,, \tag{1.3b}$$

$$S_2 \;=\; I_{+45} - I_{-45} \,, \tag{1.3c}$$

[1] We have not made an attempt to derive it explicitly. One can refer to the classic text by Born and Wolf [6] for an explanation and derivation.

$$S_3 = I_R - I_L . \tag{1.3d}$$

Since the interest often lies only in the relative values of the Stokes parameter, they can be normalised to the first parameter so that the incident beam is of unit irradiance, i.e. (S_0, S_1, S_2, S_3) becomes (1, S_1/S_0, S_2/S_0, S_3/S_0). The normalised Stokes vector can be further reduced to a three-parameter vector, by discarding the first component: (1, S_1/S_0, S_2/S_0, S_3/S_0) → (S_1, S_2, S_3) / S_0. Such a reduced Stokes vector is useful to us because its three Stokes parameters may be regarded as the Cartesian coordinates of a point in a three dimensional sphere – the Poincaré sphere. Points which fall on the surface of the sphere represent complete (i.e. pure) polarisation states. We now turn our attention to the Poincaré sphere representation of polarised light.

1.1.2. Poincaré Sphere Representation of Polarised Light

The Poincaré sphere was first introduced by Henri Poincaré in 1892. It provides a convenient way to represent polarised light and to predict how the polarisation states are changed by a given retarder. The whole Poincaré-sphere space corresponds to all the possible polarisation states of the light.

Figure 1.1 shows the three dimensional Poincaré sphere. Points on the surface of the sphere represent pure polarisation states. Those which fall on the equator correspond to linear states of polarisation. The north and south poles of the sphere represent right- and left-circular polarisation states respectively. All other points on the surface of the Poincaré sphere relate to elliptical states of polarisation. The points which fall on the inside of the sphere mark states of partial polarisation. A completely unpolarised beam will correspond to the origin of the sphere.

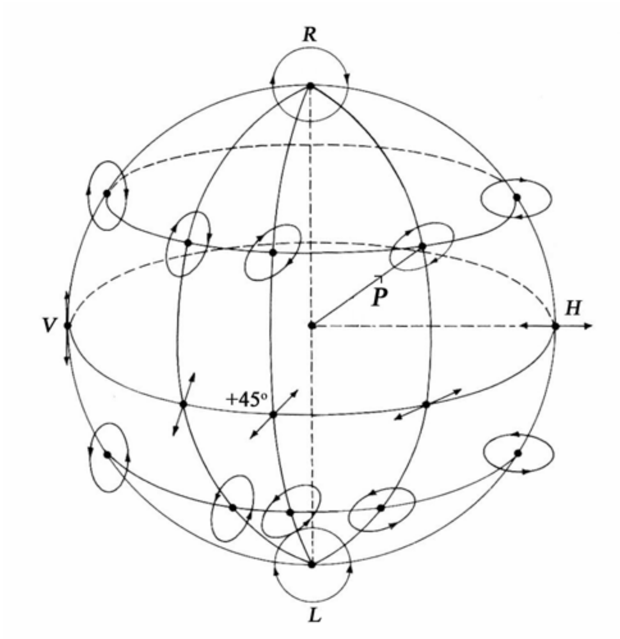

Figure 1.1: The Poincaré sphere representation of polarisation. Linearly polarised light falls on the equator, with horizontal (*H*) and vertical (*V*) polarisation states at opposite ends. Right- (*R*) and left- (*L*) circular polarisation states correspond to north and south poles respectively. The polarisation of the light can be imagined to be a vector ***P*** pointing from the origin of the sphere to the polarisation state in the sphere. Picture adapted from [7].

1.1.3. Jones Vectors

Another representation of polarised light – the Jones vector – was invented by R. Clark Jones in 1941. The Jones vector is applicable only to polarised light waves. It is a two-element column vector which makes use of the electric vector $\boldsymbol{E}$ to describe the polarisation form and the amplitude components of light:

Consider a light wave travelling in the direction of z-axis. Since there are two dimensions perpendicular to a given line of propagation, transverse wave can occur in two independent states of polarisation, which can be represented as

$$\boldsymbol{E}_x(z, t) = E_{0x} \cos(kz - wt)\, \hat{\boldsymbol{\imath}} \ , \tag{1.4a}$$

$$\boldsymbol{E}_y(z, t) = E_{0y} \cos(kz - wt + \varepsilon)\, \hat{\boldsymbol{\jmath}} \ , \tag{1.4b}$$

where ε is the relative phase difference between the waves. We can write $\boldsymbol{E}$ as

$$\boldsymbol{E} = \begin{pmatrix} E_x(t) \\ E_y(t) \end{pmatrix} . \tag{1.5}$$

Here, E_x and E_y are the instantaneous scalar components of $\boldsymbol{E}$. This can be written in the complex form in order to preserve the phase information.

$$\boldsymbol{E} = \begin{pmatrix} E_{0x} e^{i\varphi_x} \\ E_{0y} e^{i\varphi_y} \end{pmatrix} , \tag{1.6}$$

where φ_x and φ_y are the appropriate phases.

In the case where only the x-component is present, $\boldsymbol{E}(z,\ t) = \boldsymbol{E}_x(z,\ t)$, we have of course light that is horizontally polarised. Similarly, the light is vertically polarised if only the y-component is present. Thus, with normalisation, horizontal and vertical polarisation states are written as:

$$\begin{aligned} \boldsymbol{E}_H &= \begin{pmatrix} E_{0x} e^{i\varphi_x} \\ 0 \end{pmatrix} \equiv \begin{pmatrix} 1 \\ 0 \end{pmatrix} , \\ \boldsymbol{E}_V &= \begin{pmatrix} 0 \\ E_{0y} e^{i\varphi_y} \end{pmatrix} \equiv \begin{pmatrix} 0 \\ 1 \end{pmatrix} . \end{aligned} \tag{1.7}$$

Letting ε assume zero or an integral multiple of $\pm 2\pi$ in eq. (1.4), we will have

$$\begin{aligned} \boldsymbol{E}(z, t) &= \boldsymbol{E}_x (z, t) + \boldsymbol{E}_y (z, t) \\ &= (E_{0x}\, \hat{\boldsymbol{\imath}} + E_{0y} \hat{\boldsymbol{\jmath}}) \cos (kz - wt) . \end{aligned} \tag{1.8}$$

This resultant $\boldsymbol{E}$ oscillates at an angle of +45° when the light wave is seen head on. If ε is instead an odd integral multiple of $\pm\pi$, we have

$$\boldsymbol{E}(z, t) = (E_{0x}\, \hat{\boldsymbol{\imath}} - E_{0y} \hat{\boldsymbol{\jmath}}) \cos (kz - wt) , \tag{1.9}$$

which oscillates at an angle of –45°. With this knowledge, we can write the ±45° linear polarisation states in Jones vectors form:

$$\begin{aligned} \boldsymbol{E}_{+45} &= \begin{pmatrix} E_{0x} e^{i\varphi_x} \\ E_{0x} e^{i\varphi_x} \end{pmatrix} \equiv \frac{1}{\sqrt{2}} \begin{pmatrix} 1 \\ 1 \end{pmatrix} , \\ \boldsymbol{E}_{-45} &= \begin{pmatrix} E_{0x} e^{i\varphi_x} \\ -E_{0x} e^{i\varphi_x} \end{pmatrix} \equiv \frac{1}{\sqrt{2}} \begin{pmatrix} 1 \\ -1 \end{pmatrix} . \end{aligned} \tag{1.10}$$

Lastly, right- and left-circularly polarised light are the result of $\boldsymbol{E}_x$ and $\boldsymbol{E}_y$ having the same amplitude and a relative phase difference of 90°. Hence, the right- and left-circular polarisation states are given by

$$\boldsymbol{E}_R = \begin{pmatrix} E_{0x} e^{i\varphi_x} \\ E_{0x} e^{i(\varphi_x + \pi/2)} \end{pmatrix} \equiv \frac{1}{\sqrt{2}} \begin{pmatrix} 1 \\ i \end{pmatrix} ,$$
$$\boldsymbol{E}_L = \begin{pmatrix} E_{0x} e^{i\varphi_x} \\ E_{0x} e^{i(\varphi_x - \pi/2)} \end{pmatrix} \equiv \frac{1}{\sqrt{2}} \begin{pmatrix} 1 \\ -i \end{pmatrix} . \tag{1.11}$$

We note that

$$\boldsymbol{E}_{+45} = (\boldsymbol{E}_H + \boldsymbol{E}_V)/\sqrt{2} ,$$
$$\boldsymbol{E}_{-45} = (\boldsymbol{E}_H - \boldsymbol{E}_V)/\sqrt{2} , \tag{1.12}$$

$$\boldsymbol{E}_R = (\boldsymbol{E}_H + i\boldsymbol{E}_V)/\sqrt{2} ,$$
$$\boldsymbol{E}_L = (\boldsymbol{E}_H - i\boldsymbol{E}_V)/\sqrt{2} . \tag{1.13}$$

In this Jones vector formulation of polarisation states, two vectors, $\boldsymbol{A}$ and $\boldsymbol{B}$, are considered orthogonal when $\boldsymbol{A}\cdot\boldsymbol{B}^* = 0$. From eqs. (1.7), (1.10) and (1.11), observe that

$$\boldsymbol{E}_H \cdot \boldsymbol{E}_V^* = \boldsymbol{E}_{+45} \cdot \boldsymbol{E}_{-45}^* = \boldsymbol{E}_R \cdot \boldsymbol{E}_L^* = 0 . \tag{1.14}$$

The usefulness of the Jones vector formulation lies in its ability to predict the outcome of passing a polarised beam through a series of ideal optical devices by doing simple matrix-algebraic computation. Suppose that a polarised beam passes through an optical element, and the polarisation changes (in Jones vector formulation) from $\boldsymbol{E}$ to $\boldsymbol{E}'$. This transformation from $\boldsymbol{E}$ to $\boldsymbol{E}'$ can be described mathematically using a 2×2 matrix. Let $\boldsymbol{A}$ represent the transformation matrix of the optical element, and we have:

$$\boldsymbol{E}' = \boldsymbol{A}\boldsymbol{E} . \tag{1.15}$$

If the beam passes through a series of optical devices represented by the matrices $\boldsymbol{A}_1$, $\boldsymbol{A}_2$ …, $\boldsymbol{A}_n$, the resulting polarisation of the beam of light will be

$$\boldsymbol{E}' = \boldsymbol{A}_n \ldots \boldsymbol{A}_2\boldsymbol{A}_1\boldsymbol{E} . \tag{1.16}$$

The Jones matrices of a half-wave plate and a quarter-wave plate, with their fast axis vertical, are given by [8]:

$$\mathbf{HP} \equiv \begin{pmatrix} 1 & 0 \\ 0 & -1 \end{pmatrix} , \tag{1.17}$$

$$\mathbf{QP} \equiv \begin{pmatrix} 1 & 0 \\ 0 & i \end{pmatrix} . \tag{1.18}$$

1.2. Polarisation Measurement

Polarimeters are optical instruments used to determine the polarisation of light beams. Figure 1.2(a) shows a classic polarimeter. With appropriate settings for the quarter-wave plate and the half-wave plate, the linear diagonal and the circular polarisation states can be rotated such that they lie on the *H-V* polarisation axis of the Poincaré sphere. The polariser then allows only horizontally polarised light to pass through. As such, the intensity registered by the detector is that of the original polarisation states that is subsequently rotated onto the *H-V* polarisation axis. Six consecutive measurements can be taken to establish the Stokes vector, in accordance with eq (1.3):

$$\frac{S_1}{S_0} = \frac{I_H - I_V}{I_H + I_V} , \tag{1.19a}$$

$$\frac{S_2}{S_0} = \frac{I_{+45} - I_{-45}}{I_{+45} + I_{-45}} , \tag{1.19b}$$

$$\frac{S_3}{S_0} = \frac{I_R - I_L}{I_R + I_L} . \tag{1.19c}$$

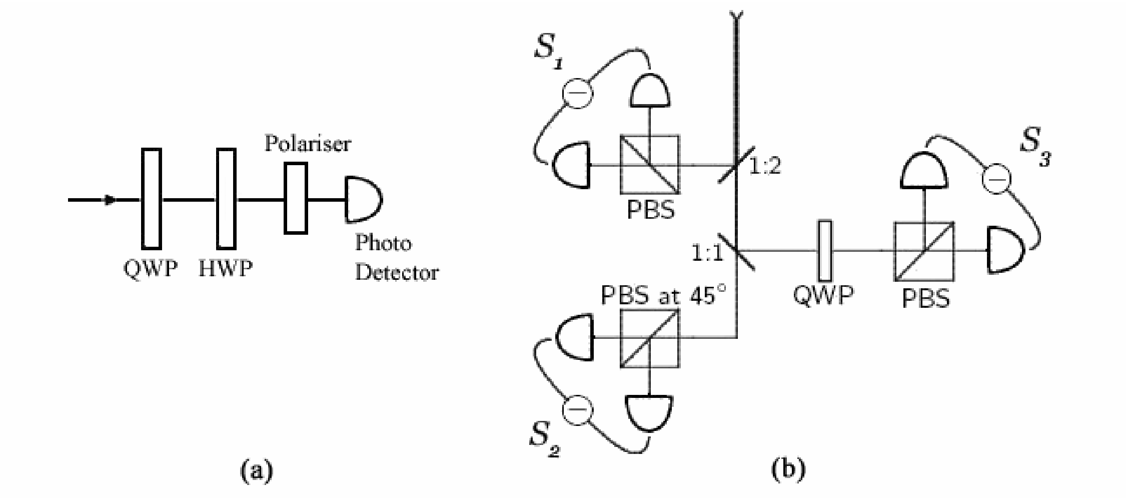

Figure 1.2 (a): A classic polarimeter. The quarter-wave plate (QWP) and the half-wave plate (HWP) rotate the polarisation of the incoming beam onto the H-V polarisation axis of the Poincaré sphere, before the horizontally polarised state passes through the polariser and hits the detector. **(b):** The six intensities needed to compute the Stokes vector can be measured simultaneously by making use of polarising beam splitters (PBS), which transmit horizontally polarised light and reflects vertically polarised light. Picture (b) adapted from [1].

Determining the Stokes parameters with this polarimeter is somewhat tedious since the two waveplates[2] have to be rotated each time a new measurement is to be taken. This can easily be avoided with the polarimeter shown in Figure 1.2(b). In this compact setup, the use of polarising beam splitters allows the six intensities to be measured simultaneously. Here, two beam splitters split the beam according to the specified ratio so that each pair of detectors gets the same share of input intensity. The polarising beam splitters (PBS) then transmit horizontally polarised light and reflect vertically polarised light. Subsequently, the polarisation of the light beam can be easily characterised by evaluating eqs. (1.19). (The PBS rotated by 45° will then transmit +45° and reflect –45° polarised light, while the quarter-wave plate placed before the last PBS converts the polarisation states: right-circular to horizontal and left-circular to vertical, so that I_R and I_L can be measured.)

[2] The general technical term for half-wave plate and quarter-wave plate is “retardation plate”. However, the usage of “waveplate” has become common. We shall continue to use this latter term for the sake of simplicity.

CHAPTER 2

Quantum State Tomography

Quantum state tomography is the process by which an unknown quantum state is fully characterised [9]. This is done by performing a series of measurement on the complimentary aspect of an ensemble of identical quantum states so that the density matrix of the state can be constructed. Its classical counterpart will be the process of three-dimensional imaging, where the subject must be scanned from different physical directions before it can reconstructed digitally.[3] Interest in measuring quantum states arises from the fact that once the state of the system is known, certain quantities which have not been (or cannot be) directly measured can be calculated [10].

In this chapter, an outline of the theory of tomography found in the articles by Řeháček *et al.* [1] and by Altepeter *et al.* [9] is given.

2.1. Representation of Single-Qubit States

In general, a single qubit in a pure state can be represented by

$$|\psi\rangle = \alpha|0\rangle + \beta|1\rangle \ , \tag{2.1}$$

[3] This analogy is taken from [9].

where $|0\rangle$ and $|1\rangle$ are two orthogonal states, and α and β are complex, with

$$|\alpha|^2 + |\beta|^2 = 1 \ . \tag{2.2}$$

The density matrix of the prepared states can, in general, be expressed as:

$$\hat{\rho} = \frac{1}{2}\sum_{i=0}^{3} s_i \cdot \hat{\sigma}_i \ , \tag{2.3}$$

where $\hat{\sigma}_i$ are the Pauli operators:

$$\hat{\sigma}_0 \equiv \begin{pmatrix} 1 & 0 \\ 0 & 1 \end{pmatrix} , \quad \hat{\sigma}_1 \equiv \begin{pmatrix} 1 & 0 \\ 0 & -1 \end{pmatrix} , \quad \hat{\sigma}_2 \equiv \begin{pmatrix} 0 & 1 \\ 1 & 0 \end{pmatrix} , \quad \hat{\sigma}_3 \equiv \begin{pmatrix} 0 & -i \\ i & 0 \end{pmatrix} , \tag{2.4}$$

and

$$s_i = \langle \hat{\sigma}_i \rangle = \mathrm{Tr}\{\hat{\sigma}_i \hat{\rho}\} \ . \tag{2.5}$$

Our desire to experimentally characterise the quantum state boils down to determine s_i with precision. Since s_i is the trace of two operators, it is a number. In our case where the qubit is encoded into the electric field polarisation of photons, s_i is just our Stokes parameter, and $|0\rangle$ and $|1\rangle$ represent horizontally and vertically polarised light respectively.

Thus, recalling the relation between the various polarisation states in eq. (1.3), we have

$$s_0 = P_{|H\rangle} + P_{|V\rangle} \ , \tag{2.6a}$$

$$s_1 = P_{|H\rangle} - P_{|V\rangle} \ , \tag{2.6b}$$

$$s_2 = P_{|+45\rangle} - P_{|-45\rangle} \ , \tag{2.6c}$$

$$s_3 = P_{|R\rangle} - P_{|L\rangle} \ , \tag{2.6d}$$

where

$$|H\rangle = |0\rangle \ , \quad |V\rangle = |1\rangle \ , \tag{2.7}$$

$$\left|\pm 45\right\rangle = \frac{1}{\sqrt{2}}\left(\left|H\right\rangle \pm \left|V\right\rangle\right) , \tag{2.8}$$

$$\left|R\right\rangle = \frac{1}{\sqrt{2}}\left(\left|H\right\rangle + i\left|V\right\rangle\right) ,$$

$$\left|L\right\rangle = \frac{1}{\sqrt{2}}\left(\left|H\right\rangle - i\left|V\right\rangle\right) , \tag{2.9}$$

and $P_{|\psi\rangle}$ is the probability getting state $|\psi\rangle$ in a measurement. Recalling what we have for classical optics, we see that $P_{|\psi\rangle}$ is of course just the intensity detected for a particular polarisation basis, i.e. $P_{|\psi\rangle}$ is obtained directly from our experiment measurements.[4]

$$P_{|\psi\rangle} = \langle\psi|\hat{\rho}|\psi\rangle = \mathrm{Tr}\{|\psi\rangle\langle\psi|\hat{\rho}\} . \tag{2.10}$$

By construction, the relationships between the various polarisation bases given by eqs. (2.8) and (2.9) are the same as what we have in Jones vectors representation of polarisation states (eqs. (1.12) and (1.13)).

Since the Stokes parameters can be used as coordinates in three-dimensional space to mark a point on the Poincaré sphere, the Poincaré sphere is now a useful tool for us to visualise single qubit state. Any state and its orthogonal partner are found on opposite points on the Poincaré sphere.

2.1.1 Minimal Qubit Tomography

Just as when we determine the Stokes parameters in §1.2., we see that six probabilities are required before the density matrix can be constructed. However, since $|0\rangle$ and $|1\rangle$ are orthogonal,

[4] Strictly speaking, the intensity detected is proportional to the probability of a measurement outcome. But we are always dealing with the relative intensities, and hence we can conveniently equate the two.

$$P_{|0\rangle} + P_{|1\rangle} = 1$$

$$\Rightarrow P_{|0\rangle} - P_{|1\rangle} = 2P_{|0\rangle} - 1 \ . \tag{2.11}$$

This is not true for just the horizontal and vertical polarisation states; it is true for other orthogonal polarisation states as well. What this implies is that instead of six probabilities, three will be sufficient for us to establish s_i. Each measurement defines a degree of freedom of the qubit in the Hilbert space, as shown in Figure 2.1. In practice, a fourth measurement is necessary for the purpose of normalisation. Thus, only four measurements are needed to construct the density matrix for single qubit. We call this minimal four-state tomography.

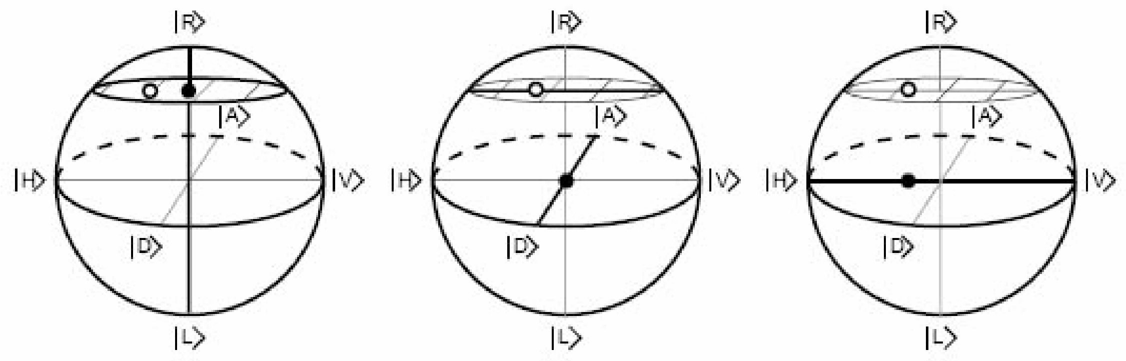

Figure 2.1: Three linearly independent measurements locate the position of the qubit (the white dot) in the Hilbert space (represented here by Poincaré sphere). The first measurement in the *R-L* basis isolates the unknown state to a plane. Subsequent measurements further isolate it to a line, and then a point. The black dot represents the projection of the qubit onto the bases. Picture adapted from [9].

Clearly, while any four measurements of linearly independent polarisation states will give us the information needed to construct the density matrix, a specific choice of four will give us the result with the least uncertainty. This has been demonstrated recently by Řeháček *et al.* [1].

Recall that in quantum mechanics, for a typical von Neumann-type projective measurement of a quantum system, all the possible measurement outcomes are represented by a set of orthogonal states $\left|a_i\right\rangle$, where a_i denotes the various possible outcomes. A measurement corresponds to a projection operator $|a_i\rangle\langle a_i|$ acting on the initial states of the system.

A more general measurement, in which the measurement operators correspond to non-orthogonal states, is given by the positive operator valued measure (POVM). A POVM is a set of positive Hermitian operators that satisfy the completeness relation:

$$\sum_j \hat{A}_j = 1 \ . \tag{2.12}$$

In a system with its state described by the statistical operator $\hat{\rho}$, the probability P_j of outcome j is given by:

$$P_j = \mathrm{Tr}\{\hat{A}_j \hat{\rho}\} \, . \tag{2.13}$$

For a set of four vectors $\{\vec{a}_j\}$ normal to the four faces of a regular tetrahedron (refer to Figure 2.2), they obey the following relation:

$$a_j \cdot a_k = \frac{4}{3}\delta_{jk} - \frac{1}{3} = \begin{cases} 1, j = k \\ -1/3, j \neq k \end{cases}, \quad \text{where } j, k = 1, 2, 3, 4. \tag{2.14}$$

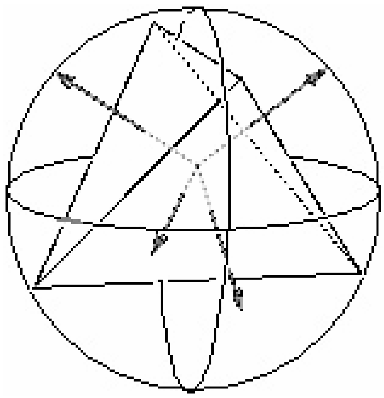

Figure 2.2: A set of four vectors normal to the faces of a regular tetrahedron, with unit amplitude, constitute a POVM. Picture adapted from [1].

This set of four vectors $\vec{a}_j$ constitutes a POVM [1] in accordance with:

$$\hat{A}_j = \frac{1}{4}\left(1 + \sum_{k=1}^{3} a_{jk}\hat{\sigma}_k\right) , \tag{2.15}$$

where a_{jk} refers to the k^{th} component of vector $\vec{a}_j$. The expression assumes a neater form if we insert a unity into the vectors $\vec{a}_j$ so that they are now four-component vectors which correspond to normalised Stokes vectors, i.e. (x,y,z) → (1, x, y, z). Then, eqs. (2.15) becomes

$$\hat{A}_j = \frac{1}{4}\sum_{k=0}^{3} a_{jk}\hat{\sigma}_k \quad , \tag{2.16}$$

and it obeys eq. (2.12)

$$\sum_{j=1}^{4} \hat{A}_j = 1 \quad . \tag{2.17}$$

Řeháček *et al.* showed that [1] for a given input state, when the average distance over all possible four-element POVMs is minimised, the end result is satisfied by any POVM of a perfect tetrahedron. In other words, the four states which will give us the least errors in the constructed density matrix corresponds to any four points on the Poincaré sphere that will form a perfect tetrahedron.

In the light of what we have brought up in this section, we note that the six-measurement polarimeters discussed in §1.2 can be classified as a form of von Neumann-type projective measurement, since the three polarisation bases used to compute the Stokes parameters are orthogonal to each other on the Poincaré sphere. The polarimeter which we built, however, is based on POVM measurement. We will be drawing parallels between the POVM of a tetrahedron and the existing optical techniques of polarimetry in the next chapter.

2.2. Representation of Pair-Qubit States

In the preceding section, what we have essentially done is to recast the standard knowledge of polarisation in classical optics into the language of quantum mechanics.

However, the formalism can be generalised to multiple qubits, and be used to investigate non-classical phenomena such as entanglement. In the following discussion, we shall focus on extending the above ideas to two-qubit systems only, since it is relevant to our experiment later.

As in the single-qubit case, the general form of a two-qubit pure state is given by

$$\left|\psi\right\rangle = \alpha\left|00\right\rangle + \beta\left|01\right\rangle + \gamma\left|10\right\rangle + \kappa\left|11\right\rangle \ , \tag{2.18}$$

where α, β, γ, κ are complex,

$$\left|\alpha\right|^2 + \left|\beta\right|^2 + \left|\gamma\right|^2 + \left|\kappa\right|^2 = 1 \ , \tag{2.19}$$

and $\left|00\right\rangle$ is the shorthand for $\left|0\right\rangle_1 \otimes \left|0\right\rangle_2$. The subscripts 1 and 2 denote qubit 1 and qubit 2.

Eq. (2.3) can be generalise to

$$\begin{aligned} \hat{\rho} &= \frac{1}{2^n}\sum_{\nu=1}^{4^n}\hat{\Gamma}_\nu S_\nu \\ &= \frac{1}{4}\sum_{\nu=1}^{16}\hat{\Gamma}_\nu S_\nu \ , \end{aligned} \tag{2.20}$$

where n is the number of qubits (n = 2 in our case). $\hat{\Gamma}$ and S are the Pauli-matrices-equivalent and Stokes-vector-equivalent for our two-qubit system. A convenient set of 16 matrices for $\hat{\Gamma}$ will be the tensor products of the Pauli matrices:

$$\hat{\Gamma}_\nu = \hat{\sigma}_i \otimes \hat{\sigma}_j \ , \quad i, j = 1, 2, 3, 4. \tag{2.21}$$

Then, the probability for the μ^{th} measurement is given by

$$\begin{aligned} P_\mu &= \left\langle \psi_\mu \right| \hat{\rho} \left| \psi_\mu \right\rangle \\ &= \left\langle \psi_\mu \right| \frac{1}{4}\sum_{\nu=1}^{16}\hat{\Gamma}_\nu S_\nu \left| \psi_\mu \right\rangle \\ &= \frac{1}{4}\sum_{\nu=1}^{16} W_{\mu,\nu} S_\nu \ , \end{aligned} \tag{2.22}$$

where $\left|\psi_\mu\right\rangle$ (μ = 1 to 16) is the measurement basis and $\boldsymbol{W}$ is a 16 × 16 matrix given by

$$W_{\mu,\nu} = \langle \psi_\mu | \hat{\Gamma}_\nu | \psi_\mu \rangle$$
$$= \mathrm{Tr}\{\hat{\Gamma}_\nu |\psi_\mu\rangle\langle\psi_\mu|\}. \tag{2.23}$$

Eq. (2.22) can be inverted to give

$$S_\nu = 4\sum_{\mu=1}^{16}\left(W^{-1}\right)_{\mu,\nu} P_\mu \quad . \tag{2.24}$$

Substituting this expression into eq. (2.20), we see that the probability density matrix we are interested in is given by

$$\hat{\rho} = \sum_{\nu=1}^{16}\sum_{\mu=1}^{16}\hat{\Gamma}_\nu \left(W^{-1}\right)_{\mu,\nu} P_\mu \quad . \tag{2.25}$$

With eq. (2.25), we have expressed $\hat{\rho}$ in a way which can be easily computed. Operator $\hat{\Gamma}_\nu$ and matrix $W_{\mu,\nu}$ can be obtained by computing the relevant tensor products, whereas P_μ, as in the case of single-qubit system, is an experimental measurement. In the present context of two-qubit system, P_μ is the coincidence count between two the detectors from two different polarimeters set up to detect incoming correlated photon pairs. Furthermore, since we will be implementing minimal state tomography, the measurement bases corresponds to the tensor products of the 4-component tetrahedron vectors of two polarimeters, $\vec{a}_i$ and $\vec{b}_j$:

$$|\psi_\mu\rangle = \vec{a}_i \otimes \vec{b}_j \ , \quad i, j = 1, 2, 3, 4. \tag{2.26}$$

Famous examples of pure two-qubit states are the Bell states:

$$\begin{aligned} |\Phi^\pm\rangle &= \frac{1}{\sqrt{2}}\left(|HH\rangle \pm |VV\rangle\right), \\ |\Psi^\pm\rangle &= \frac{1}{\sqrt{2}}\left(|HV\rangle \pm |VH\rangle\right). \end{aligned} \tag{2.27}$$

We will be generating the Bell states and attempt to reconstruct its density matrix from the detector counts.

CHAPTER 3

Minimal and Optimal Polarimetry

The schemes for the two polarimeters outlined in chapter one are motivated by the way we construct the Stokes vector. They are, however, far from being efficient since the Stokes parameters can be determined with fewer measurements. There is plainly a redundancy in the information collected.

3.1. Optimisation of Minimal Polarimeter

Indeed, taking four measurements is sufficient to establish the value of the three parameters. Such schemes are described as "minimal" because there is no excess information collected. Furthermore, much interest also lies in optimising these schemes, so as to obtain as accurate as possible a description of the light polarisation, which would be very desirable in fields which demand a high precision.

3.1.1 Maximisation of Matrix Determinant

Considerable research on the optimisation of polarimetry has been carried out [12-17], and the basic strategy common to all lies in maximising the determinant of the "instrument matrix", which is unique to the experimental setup. Recall that in §1.1.4., we introduce the Jones vectors and Jones calculus, which allow us to construct a 2 × 2 matrix representation of a system by multiplying the matrices of the optical elements of the system in the right order. We can then pre-multiply the resultant matrix to the Jones vector representation of the input state and predict the polarisation of the beam after it exits from the system of optical elements.

In 1943, Hans Mueller devised a similar method for dealing with the Stokes vectors. In this method, optical devices are characterised by 4 × 4 matrices. Since the (ratio of) intensity of the light incident on the detectors of a polarimeter is dependent on its polarisation (which is why the polarisation can be determined from the detector readings), we can formulate the expression

$$\boldsymbol{I} = \boldsymbol{K}\boldsymbol{S}_o \,, \tag{3.1}$$

where $\boldsymbol{I}$ is a 4-component vector of the intensities reading at the four output ports of a minimal polarimeter, $\boldsymbol{S}_o$ is the Stokes vector representing the light incident on the detectors, and $\boldsymbol{K}$ is a matrix which combine the Stokes parameters in the correct way to give us $\boldsymbol{I}$. However,

$$\boldsymbol{S}_o = \boldsymbol{M}_n \ldots \boldsymbol{M}_2\boldsymbol{M}_1\boldsymbol{S}_i \,, \tag{3.2}$$

where $\boldsymbol{M}_j$ is the Mueller matrix representation of the jth optical instrument which the light beam passes through before it reaches the detector, and $\boldsymbol{S}_i$ is the Stokes vector representation of the input light. Hence, we have

$$\boldsymbol{I} = \boldsymbol{K}\,\boldsymbol{M}_n \ldots \boldsymbol{M}_2\boldsymbol{M}_1\boldsymbol{S}_i = \boldsymbol{B}\boldsymbol{S}_i \,, \tag{3.3}$$

where $\boldsymbol{B} = \boldsymbol{K}\boldsymbol{M}_n \ldots \boldsymbol{M}_2\boldsymbol{M}_1$. We call matrix $\boldsymbol{B}$ the "instrument matrix".

Fortunately, the 16 elements of matrix $\boldsymbol{B}$ can be established through calibration, instead of obtaining and multiplying the Mueller matrices of all the optical devices in our setup. We will elaborate more on the determination of the instrument matrix through calibration in §4.6. For now, we just note that eq. (3.3) implies

$$\boldsymbol{S}_i = \boldsymbol{B}^{-1}\boldsymbol{I}\,. \tag{3.4}$$

According to eq. (3.4), we can extract the information of the polarisation of input light beam if we know $\boldsymbol{B}$ and measure $\boldsymbol{I}$. More importantly, eq. (3.4) tells us that an error $\delta\boldsymbol{I}$ in the measured signal I leads to a corresponding error $\delta\boldsymbol{S}$ in the derived Stokes vector [17]:

$$\delta\boldsymbol{S} = \boldsymbol{B}^{-1}\,\delta\boldsymbol{I}\,. \tag{3.5}$$

From linear algebra, we know that [18]

$$\boldsymbol{B}^{-1} = \boldsymbol{B}^{\dagger} / \det(\boldsymbol{B})\,, \tag{3.6}$$

where $\boldsymbol{B}^{\dagger}$ is the adjoint of matrix $\boldsymbol{B}$ and det($\boldsymbol{B}$) is the determinant of $\boldsymbol{B}$. Thus, we see that maximising the determinant of $\boldsymbol{B}$ is consistent with minimising $\delta\boldsymbol{S}$ [17].

3.1.2. Choice of Calibration States

We can also understand the optimisation of polarimeter from a geometrical approach. If we write the full vectors and matrix of eq. (3.3) out, we will obtain

$$\begin{pmatrix} I_1 \\ I_2 \\ I_3 \\ I_4 \end{pmatrix} = \begin{pmatrix} b_{11} & b_{12} & b_{13} & b_{14} \\ b_{21} & b_{22} & b_{23} & b_{24} \\ b_{31} & b_{32} & b_{33} & b_{34} \\ b_{41} & b_{42} & b_{43} & b_{44} \end{pmatrix} \begin{pmatrix} S_0 \\ S_1 \\ S_2 \\ S_3 \end{pmatrix}. \tag{3.7}$$

An inspection of eq. (3.7) shows that if we send in light of known polarisation states (four states needed) and measure the corresponding output intensities of each state (i.e. four sets of $\boldsymbol{S}_i$ and $\boldsymbol{I}$ are known), the elements of matrix $\boldsymbol{B}$ can be extracted by solving four sets of four simultaneous equations. If these four calibration states are represented by four points on the surface of the Poincaré sphere, our intuition tells us that the optimum choice will be four points that are as far apart as possible. (See Figure 3.1) This of course corresponds to the four vertices of a regular tetrahedron. In other words, calibration done with the vertices of a regular tetrahedron as input states will give us optimal polarimetry [13, 15]. With this in mind, we can look back at §2.1.1. and see that the optimality of a POVM of a perfect tetrahedron is consistent with our argument here.

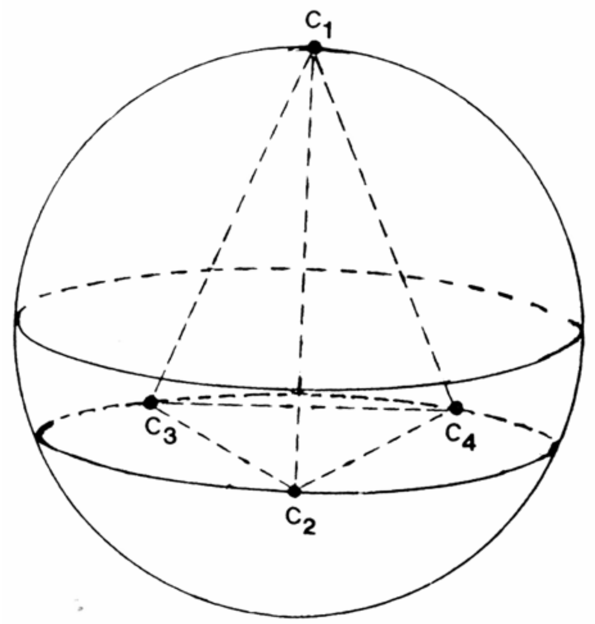

Figure 3.1: The four calibration points – C1, C2, C3 and C4 – form a skewed tetrahedron on the surface of the Poincaré sphere. The polarimeter becomes optimal when these four points are chosen to be furthest apart from each other, i.e. they form a regular tetrahedron. Determinant of the instrument matrix is proportional to the volume of this tetrahedron. Picture adapted from [13].

We note that maximising the determinant of ***B*** is equivalent to using the vertices of a regular tetrahedron as calibration states, as pointed out by Ambirajan in [15]. We mentioned in the last chapter that the relative intensities of the four detectors are the probabilities of getting a basis state in the measurement.

$$\begin{aligned} I_j = P_j &= \langle \psi_j | \hat{\rho} | \psi_j \rangle \\ &= \sum_{i=0}^{3} \frac{1}{2} \langle \psi_j | \hat{\sigma}_i | \psi_j \rangle s_i \end{aligned} \quad , \quad j = 1, 2, 3, 4, \tag{3.8}$$

where P_j is the probability of measurement in the $|\psi_j\rangle$ basis, and we substitute the expression for $\hat{\rho}$ from eq. (2.3). In the present context, the four $|\psi_j\rangle$ bases refer to the four calibration states. Comparing this with eq. (3.7) above, we observe that each row of our instrument matrix B can actually be equated to

$$\begin{aligned} B_j &= \sum_{i=0}^{3} \frac{1}{2} \langle \psi_j | \hat{\sigma}_i | \psi_j \rangle \\ &= \frac{1}{2} \sum_{i=0}^{3} \mathrm{Tr}\{ \hat{\sigma}_i | \psi_j \rangle \langle \psi_j | \}. \end{aligned} \tag{3.9}$$

However, $\mathrm{Tr}\{ \hat{\sigma}_i | \psi_j \rangle \langle \psi_j | \}$ gives us the Stokes vector for polarisation states of $|\psi_j\rangle$, as given by eq. (2.5). Thus, each row of matrix ***B*** is the transpose of the normalised Stokes vector of the calibration states (multiplied by a prefactor, which is not important to our discussion here). These Stokes vector are, in turn, the Cartesian coordinates of four points on the Poincaré sphere.

It turns out that the volume of a tetrahedron can be expressed [19] as the determinant of a 4 × 4 matrix

$$Vol_{\text{tetrahedron}} = \frac{1}{3!} \begin{vmatrix} 1 & x_1 & y_1 & z_1 \\ 1 & x_2 & y_2 & z_2 \\ 1 & x_3 & y_3 & z_3 \\ 1 & x_4 & y_4 & z_4 \end{vmatrix}, \tag{3.10}$$

with the x, y, z of each row being the coordinate of a vertices in the three dimensional space. Maximising the determinant of matrix ***B*** translates to maximising the volume of the tetrahedron, and we see that the maximum possible volume of a tetrahedron restricted to a sphere is that of a regular one.

3.2. A Review of Optimal Polarimeters

With the classic polarimeter shown in Figure 1.2(a), one can perform optimal minimal polarimetry by choosing the appropriate angles [14, 15] for the waveplates such that the calibration states are those which correspond to the vertices of a regular tetrahedron on the Poincaré sphere. The instrument matrix can then be determined and the four Stokes parameters of a beam of unknown polarisation can be computed simultaneously using eq. (3.4). However, this polarimeter is not the most convenient technique since it requires the two waveplates to be adjusted for each measurement.

An alternative approach, which involves four detectors placed such that the reflection of the light beam among these detectors is used to estimate the Stokes vector, has been demonstrated [13] by Azzam *et al.*. This method has a number of advantages over the classic polarimeter:

a) No other optical devices are required besides the four detectors. The partially reflecting surfaces of the detectors perform the function of the polarising elements in the classic polarimeter.
b) The setup has no moving parts. The polarisers of the classic polarimeter have to be rotated for each measurement.
c) The input light flux is completely utilised for polarisation determination: the last detected of the setup absorbs the light that has been reflected off the other three detectors. In the case of the classic polarimeter, only a portion of the input light flux is allowed to pass through the two waveplates. The rest is dissipated.

One should keep in mind, however, that the relative placement of the detectors is crucial for this setup. It is the key factor in this polarimeter.

Another design [17] makes use of beam splitter and prisms to achieve optimal minimal polarimetry. By including a few more optical elements, it is able to perform optimally without the stringent requirement on the relative placement of the detectors. (All the equipment must be optically aligned of course.)

The examples above are some of the developments in polarimetry in classical optics. The list of possible optical configurations for optimal minimal polarimetry is by no means exhausted. More modern means of determining light polarisation involves the use of interferometer in the polarimeter setup. Some setups need only a single loop [20], while others have more loops [1, 21]. These polarimeters also fulfil points (b) and (c) listed above, but a major drawback is that the setting up of an interferometer demands a very high degree of precision, both in the alignment of the optical elements as well as in the path length of the interferometer loop. This is a major obstacle to the practical implementation of these polarimeter schemes.

We will be constructing a polarimeter which also fulfils points (b) and (c).

CHAPTER 4

Setting Up the Polarimeter

With the tools and concepts discussed in the preceding chapters, we are now ready to present the experimental setup and the taking of tomographic measurements. Let us begin with an overview of the whole setup.

4.1. Overview

We implement the POVM of a perfect tetrahedral geometry with the setup shown in Figure 4.1. Basically, it splits the incoming beam into two portions and analyses them in different polarisation bases. The division of the beam is such that the outcome corresponds to a perfect tetrahedral geometry, thus making our polarimeter optimal. In anticipation of performing tomographic measurements on biphoton states (entangled photon pairs), we use a spontaneous parametric down converted light source[5] with a wavelength of 702 nm, collected into single mode optical fibres[6].

[5] Loosely speaking, spontaneous parametric down conversion (SPDC) is the process involving the splitting of a photon into two photons of lower energies. This process obeys the usual conservation laws, and as a result, the two photons produced are entangled. The building of a SPDC light source is outside the scope of this project and hence is not discussed here.
[6] The pairs of photon produced from the SPDC process are collected in two separate optical fibres. For single-qubit tomography, we only make use of the light in one of fibres.

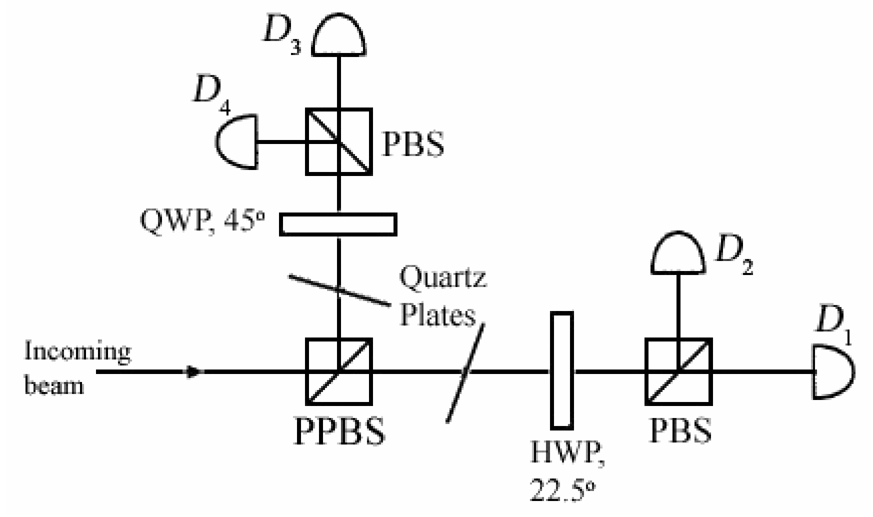

Figure 4.1: A schematic of the polarimeter setup. The incoming beam is divided into two by the partially polarising beam splitter (PPBS). The transmitted beam passes through a quartz plate at an angle, and a half-wave plate (HWP) at 22.5°, before the polarising beam splitter (PBS) sends the horizontally polarised light to detector D_1 and vertically polarised light to detector D_2. The reflected beam has to pass through a quarter-wave plate (QWP).

At the heart of this setup lies a partially polarising beam splitter (PPBS), which splits the incoming light in a certain ratio. In the Jones vector formulation, for an incoming light of polarisation $\begin{pmatrix}\alpha\\ \beta\end{pmatrix}$, the polarisation of the light along the transmitted arm after passing through the PPBS has the form $\begin{pmatrix}x\alpha\\ y\beta\end{pmatrix}$, while that along the reflected arm is $\begin{pmatrix}y\alpha\\ x\beta\end{pmatrix}$, where $x^2 = \frac{1}{2}+\frac{1}{2\sqrt{3}}$ and $y^2 = \frac{1}{2}-\frac{1}{2\sqrt{3}}$. It is this special splitting ratio which leads to the optimality of the polarimeter (as will be shown later).

The polarisation of the beam in the transmitted arm of the polarimeter is measured in the ±45° basis by letting the beam pass through a half-wave plate rotated to 22.5°. The polarising beam splitter that follows then allows horizontally polarised light to be transmitted and vertically polarised light to be reflected. (The half-wave plate causes diagonally polarised light to “rotate” to horizontally and vertically polarised light. Hence, the detectors D_1 and D_2 are in fact measuring the intensities of what was originally diagonally polarised light). Similarly, the quarter-wave plate set to 45^{o} in the reflected arm of the polarimeter allows polarisation of the beam to be measured in the right- and left-circular basis.

Silicon avalanche photodiode detectors are used because they are known to be extremely sensitive. They are connected to a computer, which has a program to count the photons detected. The counts can be collected over a time period and the data saved into the computer.

Lastly, the quartz plates along both arms are meant to compensate for the unwanted phase shift introduced by the PPBS. As shown in Figure 4.1, they are not placed perpendicular to the beam, but are rotated to an angle such that the optical path through them offset the relative phase difference.

A picture of the actual setup can be found in the appendix section.

4.2. Splitting Ratio of PPBS

We now proceed to demonstrate how the values of x and y stated above corresponds to the POVM of a tetrahedron. Let us first suppose that the polarisation of the incoming light, represented in Jones vector form, is given by $\begin{pmatrix} \alpha \\ \beta \end{pmatrix}$. After passing through the PPBS, the polarisation of the light along the transmitted arm has the form $\begin{pmatrix} x\alpha \\ y\beta \end{pmatrix}$, whereas that along the reflected arm is $\begin{pmatrix} y\alpha \\ x\beta \end{pmatrix}$. The light beams in both arms are then examined in two different polarisation bases. For a general case, we express the two orthogonal states of a polarisation basis as $\begin{pmatrix} \cos\theta \\ e^{i\phi}\sin\theta \end{pmatrix}$ and $\begin{pmatrix} -e^{-i\phi}\sin\theta \\ \cos\theta \end{pmatrix}$, and we see that the normalised light intensities along the transmitted arm are

$$\frac{I_1}{I_T} = \left| \begin{pmatrix} \cos\theta & e^{-i\varphi}\sin\theta \end{pmatrix} \begin{pmatrix} x\alpha \\ y\beta \end{pmatrix} \right|^2$$
$$= \left| x\alpha\cos\theta + y\beta e^{-i\varphi}\sin\theta \right|^2, \tag{4.1}$$

$$\frac{I_2}{I_T} = \left| \begin{pmatrix} -e^{i\varphi}\sin\theta & \cos\theta \end{pmatrix} \begin{pmatrix} xa \\ y\beta \end{pmatrix} \right|^2$$
$$= \left| -x\alpha e^{i\varphi}\sin\theta + y\beta\cos\theta \right|^2, \tag{4.2}$$

where I_1 and I_2 are the light intensities falling on detectors 1 and 2, while I_T is the total intensities of all the four detectors. Similarly, along the reflected arm, we have

$$\frac{I_3}{I_T} = \left| \begin{pmatrix} \cos\theta' & e^{-i\varphi'}\sin\theta' \end{pmatrix} \begin{pmatrix} y\alpha \\ x\beta \end{pmatrix} \right|^2$$
$$= \left| y\alpha\cos\theta' + x\beta e^{-i\varphi'}\sin\theta' \right|^2, \tag{4.3}$$

$$\frac{I_4}{I_T} = \left| \begin{pmatrix} -e^{i\varphi'}\sin\theta' & \cos\theta' \end{pmatrix} \begin{pmatrix} ya \\ x\beta \end{pmatrix} \right|^2$$
$$= \left| -y\alpha e^{i\varphi'}\sin\theta' + x\beta\cos\theta' \right|^2, \tag{4.4}$$

where I_3 and I_4 refers to the light intensities falling on detectors 3 and 4. The primed angles denote a different polarisation basis from the transmitted arm. Rearranging eq. (4.1) gives us

$$\frac{I_1}{I_T} = \left| x\alpha\cos\theta + y\beta e^{-i\varphi}\sin\theta \right|^2 = \left| \begin{pmatrix} x\cos\theta & ye^{-i\varphi}\sin\theta \end{pmatrix} \begin{pmatrix} \alpha \\ \beta \end{pmatrix} \right|^2$$
$$= \begin{pmatrix} \alpha & \beta \end{pmatrix} \begin{pmatrix} x\cos\theta \\ ye^{i\varphi}\sin\theta \end{pmatrix} \begin{pmatrix} x\cos\theta & ye^{-i\varphi}\sin\theta \end{pmatrix} \begin{pmatrix} \alpha \\ \beta \end{pmatrix}$$
$$= \langle\psi| \begin{pmatrix} x^2\cos^2\theta & xye^{-i\varphi}\sin\theta\cos\theta \\ xye^{i\varphi}\sin\theta\cos\theta & y^2\sin^2\theta \end{pmatrix} |\psi\rangle$$
$$= \left\langle \hat{A}_1 \right\rangle. \tag{4.5}$$

But recall from eq. (2.16) that the probability calculated from the POVM of a perfect tetrahedral geometry is given by:

$$\hat{A}_j = \frac{1}{4}\sum_{k=0}^{3} a_{jk}\hat{\sigma}_k \ , \tag{4.6}$$

$$\begin{aligned}
\hat{A}_1 &= \frac{1}{4}\sum_{k=0}^{3} a_{1k}\hat{\sigma}_k = \frac{1}{4}\left(a_{10}\hat{\sigma}_0 + a_{11}\hat{\sigma}_1 + a_{12}\hat{\sigma}_2 + a_{13}\hat{\sigma}_3\right) \\
&\equiv \frac{1}{4}\left[1\cdot\begin{pmatrix}1 & 0\\ 0 & 1\end{pmatrix} + a_{11}\begin{pmatrix}1 & 0\\ 0 & -1\end{pmatrix} + a_{12}\begin{pmatrix}0 & 1\\ 1 & 0\end{pmatrix} + a_{13}\begin{pmatrix}0 & -i\\ i & 0\end{pmatrix}\right] \\
&= \frac{1}{4}\begin{pmatrix}1+a_{11} & a_{12}-ia_{13}\\ a_{12}+ia_{13} & 1-a_{11}\end{pmatrix}.
\end{aligned} \tag{4.7}$$

We let $\theta = \pi/4$ and $\varphi = 0$ out of convenience. By equating eqs. (4.5) and (4.7), we have

$$\hat{A}_1 = \begin{pmatrix}x^2/2 & xy/2\\ xy/2 & y^2/2\end{pmatrix} = \frac{1}{4}\begin{pmatrix}1+a_{11} & a_{12}-ia_{13}\\ a_{12}+ia_{13} & 1-a_{11}\end{pmatrix}, \tag{4.8}$$

$$\Rightarrow \ a_{11} = x^2 - y^2\,, \quad a_{12} = 2xy\,, \quad a_{13} = 0\,. \tag{4.9}$$

Following a similar approach, we obtain

$$a_{21} = x^2 - y^2\,, \quad a_{22} = -2xy\,, \quad a_{23} = 0\,, \tag{4.10}$$

$$a_{31} = y^2 - x^2\,, \quad a_{32} = 0\,, \quad a_{33} = 2xy\,, \tag{4.11}$$

$$a_{41} = y^2 - x^2\,, \quad a_{42} = 0\,, \quad a_{43} = -2xy\,, \tag{4.12}$$

where we have set $\theta' = \pi/4$ and $\varphi' = \pi/2$. Hence,

$$\left.\begin{matrix}\vec{a}_1\\ \vec{a}_2\end{matrix}\right\} = \begin{pmatrix}x^2-y^2\\ \pm 2xy\\ 0\end{pmatrix}, \quad \left.\begin{matrix}\vec{a}_3\\ \vec{a}_4\end{matrix}\right\} = \begin{pmatrix}y^2-x^2\\ 0\\ \pm 2xy\end{pmatrix}. \tag{4.13}$$

By evaluating the dot product of these vectors and invoking eq. (2.14) as a constraint, we obtain a set of simultaneous equations:

$$\begin{aligned}
\vec{a}_1\cdot\vec{a}_2 &= \left(x^2-y^2\right)^2 - 4x^2y^2 = -1/3, \\
&\Rightarrow x^4 + y^4 - 6x^2y^2 = -1/3,
\end{aligned} \tag{4.14}$$

$$\begin{aligned}
\vec{a}_1\cdot\vec{a}_3 &= \left(x^2-y^2\right)\left(y^2-x^2\right) = -1/3, \\
&\Rightarrow 2x^2y^2 - x^4 - y^4 = -1/3.
\end{aligned} \tag{4.15}$$

It is easy to verify that

$$x^2 = \frac{1}{2} + \frac{1}{2\sqrt{3}} \ , \tag{4.16a}$$

and

$$y^2 = \frac{1}{2} - \frac{1}{2\sqrt{3}} \ , \tag{4.16b}$$

is one of the possible sets of solutions to the simultaneous equations above. This implies that a setup having a beam splitter which splits an incoming beam in the way specified above, with the values of x and y given by eq. (4.16), corresponds to the POVM of a perfect tetrahedron, i.e. the polarimeter will be minimal and optimal.

Hence, a PPBS with this special splitting ratio is ordered for the purpose of this experiment.

It should be noted that eq. (4.16) is not a unique solution which one can extract from eqs. (4.14) and (4.15). Other solutions will correspond to a tetrahedron of different orientation, which is also optimal.[7]

Another point is that the values of x and y are also dependent on the choice bases in which we measure the polarisation. Here, we set $\theta = \pi/4$, $\varphi = 0$, and $\theta' = \pi/4$, $\varphi' = \pi/2$ out of convenience and they correspond to $\pm 45^{\circ}$ basis and right/left circular basis respectively. We will have to measure the polarisation in these two bases, since the values of x and y we obtained follow from the choice of polarisation bases.

4.3. Alignment of Optical Elements

The light beam coming out from the optical fibre connected to a SPDC light source is diverging and has to be collimated (made parallel) first, before passing it through the optical elements. This can be accomplished using a lens of suitable focal length. After the beam is divided into four portions by the beam splitters, they are fed into the

[7] On a practical note, limitations in the manufacturing of partially polarising beam splitter can restrict the number of sets of solutions that can actually be realised experimentally.

detectors via optical fibres. Here, we need to focus the beams onto the optical fibres, which can be accomplished using the same lens.

4.3.1. The Lens Units

The lens is fitted inside a tube and mounted onto a holder, as shown in Figure 4.2a. The position of the lens in the tube can be shifted so that the when the optical fibre are attached to the holder too, the end of the fibre is at the focal point of the lens. The final lens unit will allow us to collimate a diverging beam coming out of an optical fibre as well as focus a collimated beam onto a fibre.

Since the beam we are using is not visible to the naked eye, we switch to a helium-neon (He-Ne) laser source for the purpose of collimating the beam and aligning the optical devices.

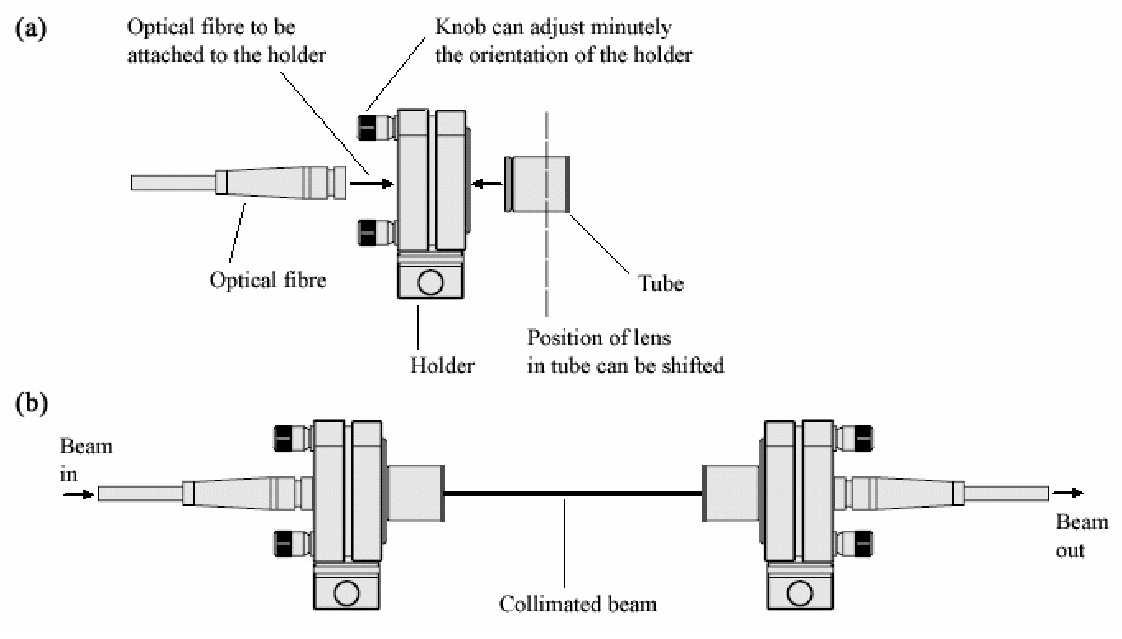

Figure 4.2(a): A lens unit. **(b):** When the beam is collimated, the cross section of the beam should have the same diameter at any position along its path. Once the lens units are aligned, the collimated laser beam will pass straight through. The beam coming out at the end will be fed into the detector.

The He-Ne laser operates in the red at 632.8 nm. The beam produced is also not directly visible, but by placing a piece of paper in its path, the profile of the beam is captured on the paper. By sending a He-Ne laser beam through an optical fibre connected to the lens unit, we know that the lens is in the right position when the beam coming out has the same cross-section area at any place along its path. (Refer to Figure 4.2b.)

Five such units are assembled – one to be connected to the SPDC source, the rest to be connected to a detector each.

4.3.2. Aligning through Maximising Output Intensity

Next, we need to align all the five units optically. In other words, we want to ensure that the collimated beam coming out of a lens unit does finally hit the lens of the remaining four units and is fed into their optical fibres.

The lens units and the beam splitters are placed on the optical bench and arranged according to the schematic shown in Figure 4.3. Then, with a piece of paper positioned in the path of the beam, the beam profile is captured and we can follow the course of the beam and ensure that it hits the lens units that will be connected to detectors.

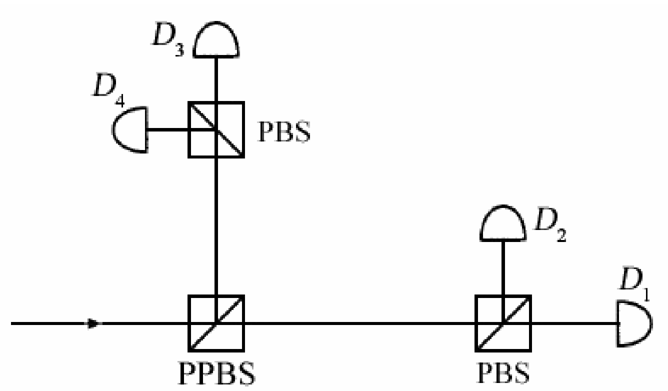

Figure 4.3: Initial setup to be aligned. D_1, D_2, D_3 and D_4 are the lens units connected to the detectors.

To ensure that the beam will indeed enter the optical fibre, we need to verify for ourselves that light leaves the other end of the fibre. For this purpose, we point the end of the fibre towards a piece of paper and check for the tell-tale sign of a red spot.

Having seen it, we will then tune the adjustment knobs on the lens holder (see Figure 4.2a). This has the effect of changing the orientation of the lens unit by minute degrees. By changing turning the knobs, we are effectively adjusting the amount of light that enters the optical fibre. Once the intensity of the red dot shown on the paper is at its highest, we connect the lens unit to a detector (which is in turn connected to a computer).

Finally, we switch back to the 702 nm wavelength beam from SPDC process and start the counter program in the computer. We now tune the adjustment knobs of the lens units again, until we are fully satisfied that the counts registered by each detector are at their maximum.

The aligning of the detectors to the beam from the source is a somewhat tedious process, but its importance cannot be overemphasised. Remember that we are using the ratio of the counts from the four detectors to reconstruct the Stokes vector of the input polarisation state. Failing to align them properly will mean that one (or more) of the detectors has counts that are less than what they should be. This will in turn affect the accuracy of our final results.

4.4. Polarisation Measurements in Two Different Bases

After the PPBS divides the incoming beam into two portions, we want to project and measure the polarisation of the transmitted beam and reflected beam in two different polarisation bases. When we compute the splitting ration of the PPBS earlier, we choose $\theta = \pi/4$, $\varphi = 0$ for one basis, and $\theta' = \pi/4$, $\varphi' = \pi/2$ for the other. These two bases correspond to $\pm 45^{\circ}$ basis and right/left circular basis respectively.

To see that this is so, we just need to substitute these angles back to the general form of orthogonal basis $\begin{pmatrix} \cos\theta \\ e^{i\phi}\sin\theta \end{pmatrix}$ and $\begin{pmatrix} -e^{-i\phi}\sin\theta \\ \cos\theta \end{pmatrix}$. With $\theta = \pi/4$ and $\varphi = 0$, the set of basis becomes $\frac{1}{\sqrt{2}}\begin{pmatrix} 1 \\ 1 \end{pmatrix}$ and $-\frac{1}{\sqrt{2}}\begin{pmatrix} 1 \\ -1 \end{pmatrix}$, which are just our ±45^o polarisation states in Jones vector formulation. Similarly, $\theta' = \pi/4$ and $\varphi' = \pi/2$ give us our right- and left-circular polarisation states: $\frac{1}{\sqrt{2}}\begin{pmatrix} 1 \\ i \end{pmatrix}$ and $\frac{i}{\sqrt{2}}\begin{pmatrix} 1 \\ -i \end{pmatrix}$.

4.4.1. Angles of Half-wave Plate and Quarter-wave Plate

In order to do a measurement in the ±45^o polarisation basis, we will need to place a half-wave plate – with its fast axis turned to 22.5^o – in the path of the beam in the transmitted arm. This half-wave plate will rotate the ±45^o polarisation states to the *H-V* polarisation basis, so that they can be divided and analysed by the polarising beam splitter and the detectors respectively.

Similarly, a quarter-wave plate with its fast axis at 45^o will rotate right- and left-circular polarisation states to *H-V* polarisation states. We can easily verify this for ourselves. Recall the Jones matrices for half-wave plate and quarter-wave plate given in eqs. (1.17) and (1.18). When a half-wave plate is rotated about it principal axis to an arbitrary angle, its new Jones matrix is

$$\begin{aligned} \mathbf{R}_{\mathrm{HWP}} &= \mathbf{R}\cdot\mathbf{HP}\cdot\mathbf{R}^{-1} \\ &= \begin{pmatrix} \cos\theta & \sin\theta \\ -\sin\theta & \cos\theta \end{pmatrix}\begin{pmatrix} 1 & 0 \\ 0 & -1 \end{pmatrix}\begin{pmatrix} \cos\theta & -\sin\theta \\ \sin\theta & \cos\theta \end{pmatrix} \\ &= \begin{pmatrix} \cos 2\theta & -\sin 2\theta \\ -\sin 2\theta & -\cos 2\theta \end{pmatrix}, \end{aligned} \tag{4.17}$$

where **R** is the rotation matrix and θ is the angle of the half-wave plate. Setting θ = 22.5°, and pre-multiplying the matrix to Jones vector of ±45° polarisation states given by eq. (1.10), we have

$$\begin{aligned} &\frac{1}{\sqrt{2}}\begin{pmatrix} 1 & -1 \\ -1 & -1 \end{pmatrix}\cdot\frac{1}{\sqrt{2}}\begin{pmatrix} 1 \\ 1 \end{pmatrix}=\begin{pmatrix} 0 \\ -1 \end{pmatrix}, \\ &\frac{1}{\sqrt{2}}\begin{pmatrix} 1 & -1 \\ -1 & -1 \end{pmatrix}\cdot\frac{1}{\sqrt{2}}\begin{pmatrix} 1 \\ -1 \end{pmatrix}=\begin{pmatrix} 1 \\ 0 \end{pmatrix}. \end{aligned} \tag{4.18}$$

From eq. (1.7), we know that these are just our *H-V* polarisation states.

For quarter-wave plate, we have

$$\begin{aligned} \mathbf{R}_{\mathrm{QWP}} &= \begin{pmatrix} \cos\varphi & \sin\varphi \\ -\sin\varphi & \cos\varphi \end{pmatrix}\begin{pmatrix} 1 & 0 \\ 0 & i \end{pmatrix}\begin{pmatrix} \cos\varphi & -\sin\varphi \\ \sin\varphi & \cos\varphi \end{pmatrix} \\ &= \begin{pmatrix} \cos^2\varphi + i\sin^2\varphi & (-1+i)\sin\varphi\cos\varphi \\ (-1+i)\sin\varphi\cos\varphi & \sin^2\varphi + i\cos^2\varphi \end{pmatrix}, \end{aligned} \tag{4.19}$$

with φ as the angle of the quarter-wave plate. When φ = 45°,

$$\begin{aligned} &\frac{1}{2}\begin{pmatrix} 1+i & -1+i \\ -1+i & 1+i \end{pmatrix}\cdot\frac{1}{\sqrt{2}}\begin{pmatrix} 1 \\ i \end{pmatrix}=\frac{-1+i}{\sqrt{2}}\begin{pmatrix} 0 \\ 1 \end{pmatrix}, \\ &\frac{1}{2}\begin{pmatrix} 1+i & -1+i \\ -1+i & 1+i \end{pmatrix}\cdot\frac{1}{\sqrt{2}}\begin{pmatrix} 1 \\ -i \end{pmatrix}=\frac{1-i}{\sqrt{2}}\begin{pmatrix} 1 \\ 0 \end{pmatrix}, \end{aligned} \tag{4.20}$$

which are, again, just our *H-V* polarisation states. We can ignore the pre-factor which denotes a global phase shift.

4.4.2. Aligning the Optical Axis of Retardation Plates

The waveplates are mounted onto a circular rotating plate which has markings at each degree interval. To set the waveplates to the desired angles, we must first align the optical axis of the plates to coincide with the vertical or horizontal axis[8]. This is done with the setup shown in Figure 4.4, which consists of two Glan-Thompson polarisers.

[8] Perpendicular axes result in polarisation states that are different from each other by just an overall phase factor, which will not affect the overall physical outcome of the experiment.

A laser diode sends a beam with wavelength of 690 nm to the first Glan-Thompson polariser. A Glan-Thompson polariser, when placed upright, will transmit horizontally polarised light while reflecting vertically polarised light. We placed the first polariser upright while rotate the second by 90^{o} (i.e., placed it on its side). This second polariser will transmit vertically polarised light and reflect horizontally polarised light. Hence, as it stands, no light will be observed coming out from the transmission port of the second Glan-Thompson polariser[9].

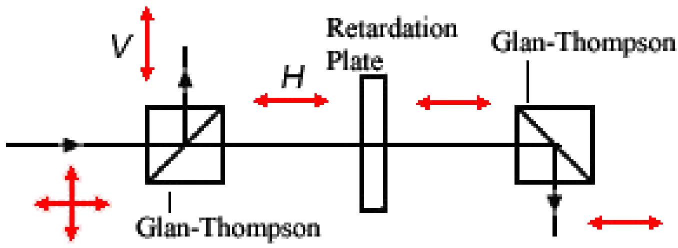

Figure 4.4: Setup for aligning optical axis of retardation plates. Red arrows represent the polarisation states. The second Glan-Thompson polariser is rotated 90^{o} so that it now transmits vertically polarised light (V). Only when the optical axis of the polarisation plate is properly aligned will it allow the horizontally polarised light (H) to pass through unchanged. Otherwise, the beam leaving the plate will have a vertical component, which will be transmitted by the second Glan-Thompson polariser.

Next, we insert the waveplate between the two Glan-Thompson polarisers. If the optical axis of the plate is vertical or horizontal, it will allow the transmitted horizontally polarised light from the first polariser to pass through unchanged. But this light will be reflected by the second polariser and hence, no light is transmitted through. For any other angle the optical axis makes with the vertical, the horizontally polarised beam from the first polariser will be rotated and acquire a vertical component, which can be transmitted through the second polariser.

[9] This can be easily verified by placing a piece of paper after the second polarizer and see if a red spot – the profile of the beam – is captured on it.

Thus, with the waveplate placed between the two Glan-Thompson polarisers, we rotate the waveplate to a position where we do not observe any light coming out from the transmission port of the second polariser.

With the optical axis aligned, we then rotate the waveplate by the desired angle – 22.5^{o} for half-wave plate and 45^{o} for quarter-wave plate. The half-wave plate is then inserted into the transmission arm of the polarimeter, while the quarter-wave plate the reflected arm (Refer back to Figure 4.1 for their position.).

4.5. Phase Correction: Quartz Plate

The polarimeter is almost complete now. The last thing we need to do is to compensate for the phase retardation introduced by the PPBS. This phase shift will give us a systematic error is left uncorrected.

4.5.1. Phase Retardation by Birefringent Quartz Plates

To change the phase difference between the two orthogonal components of the electric field of the light, $\boldsymbol{E}_x$ and $\boldsymbol{E}_y$, we need a birefringent plate. A birefingent material exhibits reflective indices which are dependent on the direction of the light passing through it. The reflective index of the birefringent plate will appear different for $\boldsymbol{E}_x$ and $\boldsymbol{E}_y$. As a result, $\boldsymbol{E}_x$ and $\boldsymbol{E}_y$ will travel at different speed and an overall phase retardation is induced in the emerging beam.

The phase change, $\Delta\delta$, is given [5] by

$$\Delta\delta = \frac{2\pi}{\lambda_0} d\left|n_o - n_e\right| \ , \tag{4.21}$$

where λ_0 is the wavelength of the light in vacuum, d is the geometrical path length taken by the light through the crystal, n_o and n_e are the two principal indices of refraction.

The birefringent property of quartz plate makes it a suitable candidate to correct for the phase shift. We first align the optical axis of a pair of quartz plates[10] and insert them into the transmitted and reflected arms of the polarimeter, as shown in Figure 4.1. They are the first optical elements in the two arms of the polarimeter so that the phase retardation due to the PPBS can be corrected first before the two beams make their way through the remaining optical elements in our setup.

As the eq. (4.21) suggests explicitly, the phase retardation induced by a birefringent material is dependent on the length of the geometrical path of light through it. By rotating the quartz plates about their optical axes, we are effectively changing the geometrical path length of the light through the quartz plate (see Figure 4.5). Hence, whatever the amount of phase shift introduced by the PPBS is, we can correct for it by turning the quartz plates through a suitable angle. We stop rotating when the phase retardation is exactly compensated for.

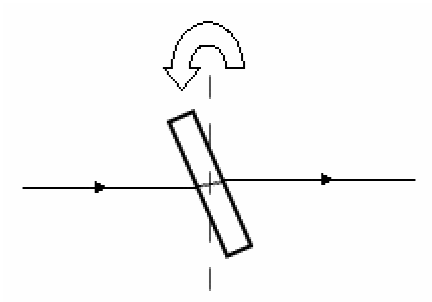

Figure 4.5: View of quartz plate from the top. By rotating it, we are effectively changing the geometrical path length of the light through it.

In order to know how much to turn the quartz plate, we have to compare the theoretical expected counts of each detector with the experimental reality. In other words, we have to send in known polarisation states and see if the behaviour of the polarimeter agrees with our own predictions.

[10] This involves the same setup and process outlined in the previous section, §4.2.2.

4.5.2. Modelling of Detectors Counts

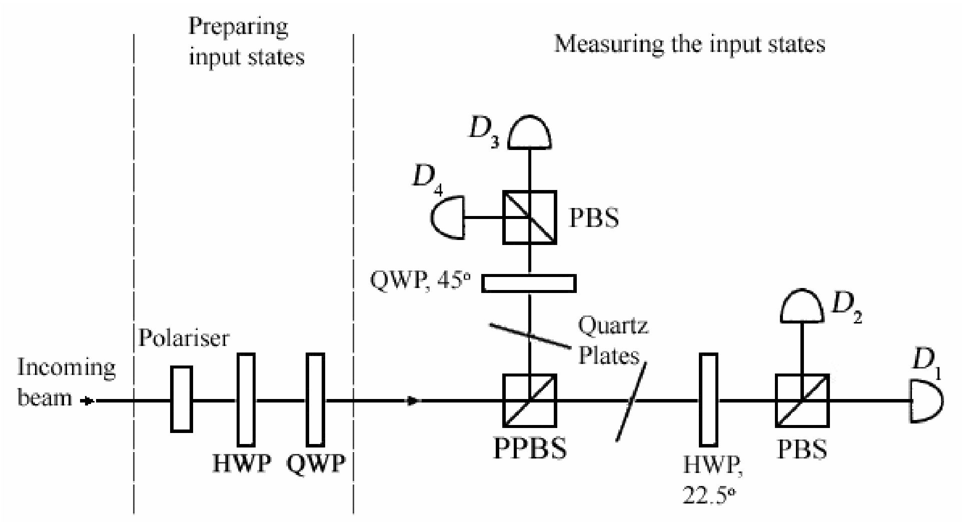

Figure 4.6: Setup for generating the input states. The half-wave plate (HWP) and quarter-wave plate (QWP) at the front can rotate the polarisation state of the incoming beam to any other possible states.

Consider the setup of Figure 4.6. We prepare the input states by placing a polariser, a half-wave plate and a quarter-wave plate in front of the polarimeter setup. The polariser will allow only horizontally polarised light to pass through. With the combination of half-wave plate and quarter-wave plate, we can then rotate the horizontally polarised light to any other possible polarisation states. On the Poincaré sphere, we are just effectively shifting a point on the equator to any other points on the surface of the sphere. The polarisation of the light that leaves these polariser plates is known because we can easily compute it using the Jones calculus.

We have already computed the general Jones matrices for half-wave plate and quarter-wave plate in eqs. (4.17) and (4.19). From eq. (1.7), we know the Jones vector of horizontally polarised light to be $\begin{pmatrix} 1 \\ 0 \end{pmatrix}$. Hence, the polarisation of light exiting the polariser wave-plates is

$$\left|\text{prep}\right\rangle \equiv \mathbf{R}_{\text{QWP}} \cdot \mathbf{R}_{\text{HWP}} \cdot \begin{pmatrix} 1 \\ 0 \end{pmatrix}, \tag{4.22}$$

where $|\text{prep}\rangle$ denotes the polarisation state prepared by us.

If we rotate the half-wave plate through a range of 360° while keeping the quarter-wave plate angle unchanged (i.e. $\varphi = 0$), we get

$$|\text{prep}\rangle = \begin{pmatrix} 1 & 0 \\ 0 & i \end{pmatrix} \begin{pmatrix} \cos 2\theta & -\sin 2\theta \\ -\sin 2\theta & -\cos 2\theta \end{pmatrix} \begin{pmatrix} 1 \\ 0 \end{pmatrix} = \begin{pmatrix} \cos 2\theta \\ -i\sin 2\theta \end{pmatrix}. \tag{4.23}$$

After passing through the PPBS, the Jones vector along the transmitted arm acquires factors of x and y:

$$\begin{pmatrix} \cos 2\theta \\ -i\sin 2\theta \end{pmatrix} \mapsto \begin{pmatrix} x\cos 2\theta \\ -iy\sin 2\theta \end{pmatrix}, \tag{4.24}$$

where we recall that $x^2 = \frac{1}{2} + \frac{1}{2\sqrt{3}} \approx 0.7887$ and $y^2 = \frac{1}{2} - \frac{1}{2\sqrt{3}} \approx 0.2113$. The half-wave plate set at 22.5° (substitute θ = 22.5° into eq. (4.17) to get the matrix) further rotate the polarisation state to

$$|\text{transmit}\rangle = \frac{1}{\sqrt{2}} \begin{pmatrix} 1 & -1 \\ -1 & -1 \end{pmatrix} \begin{pmatrix} x\cos 2\theta \\ -iy\sin 2\theta \end{pmatrix} = \frac{1}{\sqrt{2}} \begin{pmatrix} x\cos 2\theta + iy\sin 2\theta \\ -x\cos 2\theta + iy\sin 2\theta \end{pmatrix}. \tag{4.25}$$

The Jones vector along the reflected arm, on the other hand, acquires factors of y and x after the PPBS:

$$\begin{pmatrix} \cos 2\theta \\ -i\sin 2\theta \end{pmatrix} \mapsto \begin{pmatrix} y\cos 2\theta \\ -ix\sin 2\theta \end{pmatrix}, \tag{4.26}$$

which is then rotated by the quarter-wave plate at 45° (i.e. φ = 45° in eq. (4.19)):

$$|\text{reflect}\rangle = \frac{1}{2} \begin{pmatrix} 1+i & -1+i \\ -1+i & 1+i \end{pmatrix} \begin{pmatrix} y\cos 2\theta \\ -ix\sin 2\theta \end{pmatrix} = \frac{1}{2} \begin{pmatrix} y\cos 2\theta + x\sin 2\theta + iy\cos 2\theta + ix\sin 2\theta \\ -y\cos 2\theta + x\sin 2\theta + iy\cos 2\theta - ix\sin 2\theta \end{pmatrix}. \tag{4.27}$$

The ratio of counts in the four detectors can be easily calculated:

$$\begin{aligned} P_1 &= \left|\langle H \,|\, \text{transmit}\rangle\right|^2 = \left|\langle \text{transmit} \,|\, H\rangle\langle H \,|\, \text{transmit}\rangle\right| \\ &= \frac{1}{2}(x\cos 2\theta - iy\sin 2\theta)(x\cos 2\theta + iy\sin 2\theta) \\ &= \frac{1}{2}\left(x^2\cos^2 2\theta + y^2\sin^2 2\theta\right), \end{aligned} \tag{4.28}$$

where we multiply a $\langle H|$ to $|\text{transmit}\rangle$ because the polarising beam splitter allows horizontally polarised light to pass straight through to reach detector 1, while it reflects vertically polarised light to detector 2. Thus, for detector 2, we have

$$\begin{aligned} P_2 &= \left|\langle V \,|\, \text{transmit}\rangle\right|^2 \\ &= \frac{1}{2}(-x\cos 2\theta - iy\sin 2\theta)(-x\cos 2\theta + iy\sin 2\theta) \\ &= \frac{1}{2}\left(x^2\cos^2 2\theta + y^2\sin^2 2\theta\right). \end{aligned} \tag{4.29}$$

Similarly,

$$\begin{aligned} P_3 &= \left|\langle H \,|\, \text{reflect}\rangle\right|^2 \\ &= \frac{1}{2}(y\cos 2\theta + x\sin 2\theta)^2 , \end{aligned} \tag{4.30}$$

$$\begin{aligned} P_4 &= \left|\langle V \,|\, \text{reflect}\rangle\right|^2 \\ &= \frac{1}{2}(-y\cos 2\theta + x\sin 2\theta)^2 . \end{aligned} \tag{4.31}$$

A plot of the counts ratio against the angle of the half-wave plate is shown in Figure 4.7. We note that the predicted counts of detector 1 and 2 are the same.

We repeat the above analysis, this time on a similar setup except that there is no quarter-wave plate after the half-wave plate. With this setup, we have

$$|\text{prep}\rangle = \begin{pmatrix} \cos 2\theta \\ -\sin 2\theta \end{pmatrix} , \tag{4.32}$$

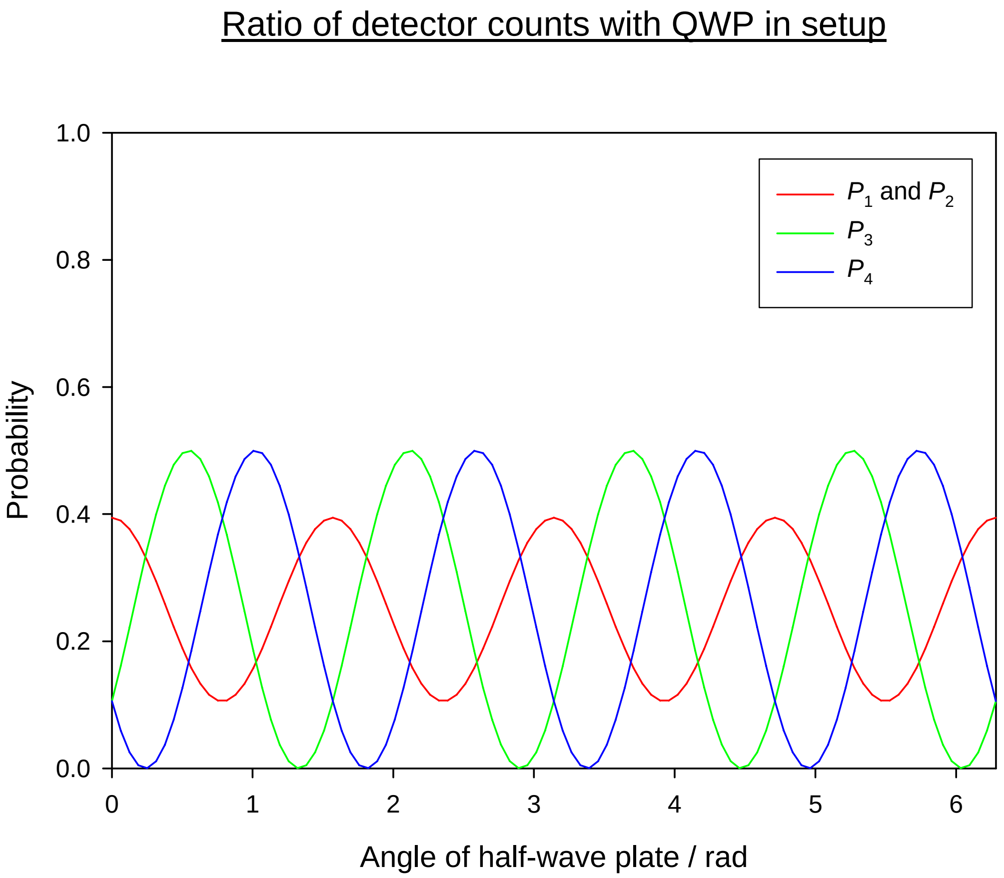

Figure 4.7: Graph of P_1, P_2, P_3 and P_4 against half-wave plate angle, with a quarter-wave plate in the setup. Plot of P_1 and P_2 coincides.

$$\begin{aligned}|\text{transmit}\rangle &= \frac{1}{\sqrt{2}}\begin{pmatrix}1 & -1\\ -1 & -1\end{pmatrix}\begin{pmatrix}x\cos 2\theta\\ -y\sin 2\theta\end{pmatrix}\\ &= \frac{1}{\sqrt{2}}\begin{pmatrix}x\cos 2\theta + y\sin 2\theta\\ -x\cos 2\theta + y\sin 2\theta\end{pmatrix},\end{aligned} \tag{4.33}$$

$$\begin{aligned}|\text{reflect}\rangle &= \frac{1}{2}\begin{pmatrix}1+i & -1+i\\ -1+i & 1+i\end{pmatrix}\begin{pmatrix}y\cos 2\theta\\ -x\sin 2\theta\end{pmatrix}\\ &= \frac{1}{2}\begin{pmatrix}y\cos 2\theta + x\sin 2\theta + iy\cos 2\theta - ix\sin 2\theta\\ -y\cos 2\theta - x\sin 2\theta + iy\cos 2\theta - ix\sin 2\theta\end{pmatrix}.\end{aligned} \tag{4.34}$$

And the ratio of the detectors counts is

$$P_1 = \frac{1}{2}(x\cos 2\theta + y\sin 2\theta)^2 \ , \tag{4.35}$$

$$P_2 = \frac{1}{2}(-x\cos 2\theta + y\sin 2\theta)^2 \ , \tag{4.36}$$

$$P_3 = P_4 = \frac{1}{4}\left[(y\cos 2\theta + x\sin 2\theta)^2 + (y\cos 2\theta - x\sin 2\theta)^2\right]. \tag{4.37}$$

We observe that the counts for detectors 3 and 4 should coincide, as shown in Figure 4.8.

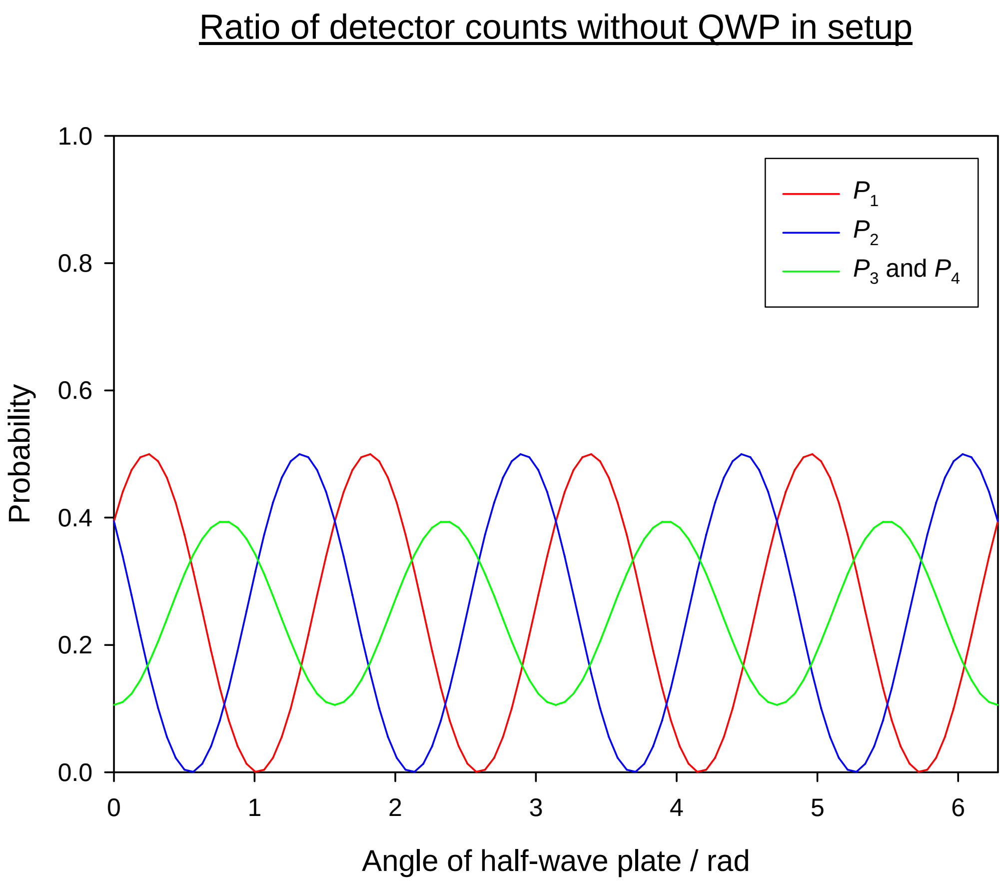

Figure 4.8: Graph of P_1, P_2, P_3 and P_4 against half-wave plate angle, without a quarter-wave plate in the setup. Plot of P_3 and P_4 coincides.

4.5.3. Dark Counts

Before we proceed with the testing of our model against the experimental results, we need to point out that our detectors will register photon counts even when the laser is switched off. We call them dark counts, since these counts represent the background light detected. They will contribute an error to our final ratio of detector counts if not taken into account. Therefore, before we start taking any measurement, we always close the aperture of the argon laser and take the readings of the dark counts for all detectors. (The dark counts registered by the detectors are dependent on their efficiency, and hence not the same for all the detectors.) These readings will then be subtracted from the subsequent data we take for the experiment.

4.5.4. Rotating the Quartz Plates

Knowing what we *should* be expecting from the detector counts, we proceed to rotate the quartz plate until reality matches our expectation. With the polariser and two retardation plates inserted in order to prepare the input states, we first leave the quarter-wave plate alone while we connect the half-wave plate to a motor and set it to rotate through a range of 360^o. At intervals of 2^o, the motor will pause for 5 seconds, allowing the detectors to take the photon counts. At the end of the 360^o turn, the photon counts of each detector are plotted against the angle of the half-wave plate.

Adopting a trial-and-error approach, we rotate the quartz plate in the transmitted arm by a small angle and repeat the data-taking procedure outlined above to check if the plot for detectors 1 and 2 coincide as they should. This step is taken repeatedly until the experimental results match with our theoretical predictions.

Next, we remove the quarter-wave plate from the setup and rotate the half-wave plate through one full turn again, collecting detector readings for 5 seconds at every 2^o interval. Without the quarter-wave plate, the plot of detector counts for detector 3 and 4 (in the reflected arm) should coincide. Hence, we rotate the quartz plate in the reflected arm until the experimental results agree with our expectation.

Figure 4.9 and 4.10 shows the experimental with the theoretical plots. The difference in amplitude between the experimental and theoretical plots is due to the efficiencies of the detectors.

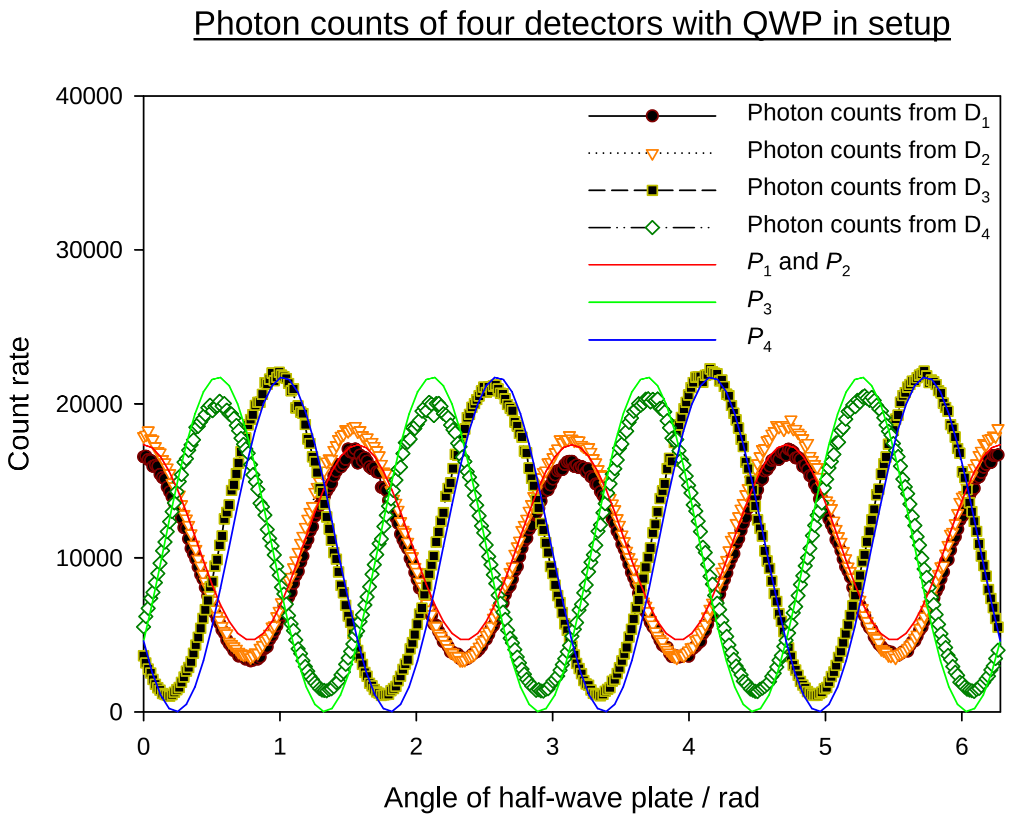

Figure 4.9: Plot of counts from four detectors with the theoretical probabilities, with the quarter-wave plate in setup. The differences in amplitude are due to the efficiencies of the detectors.

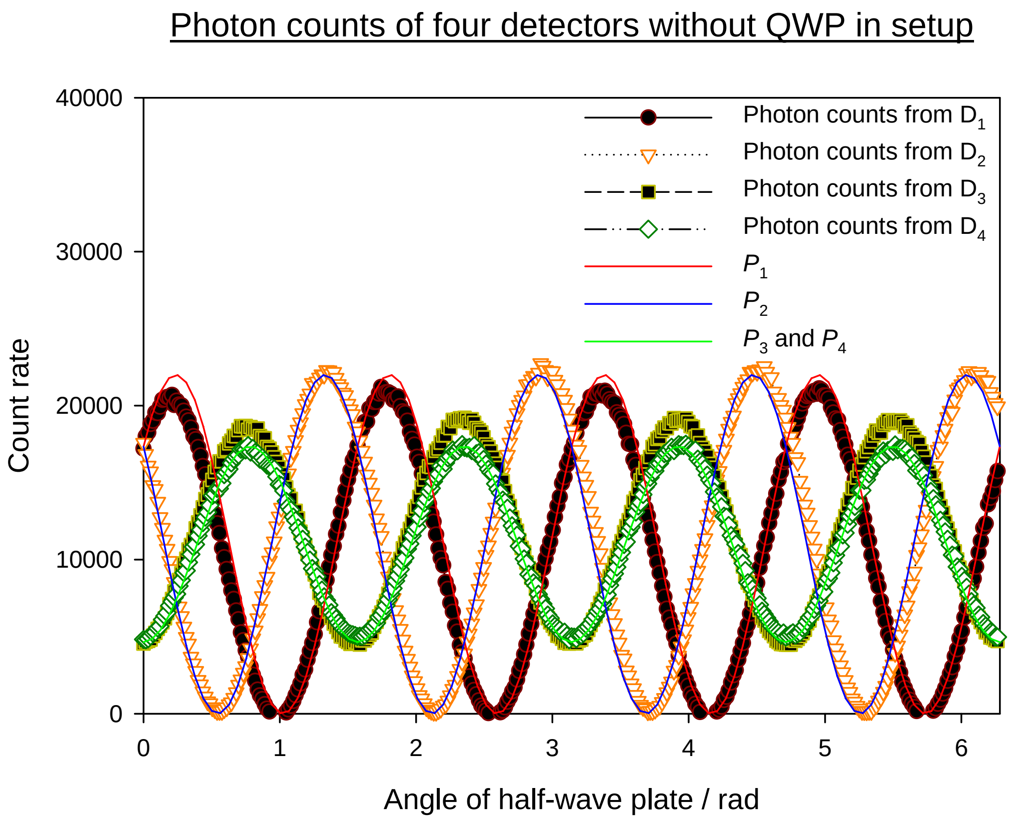

Figure 4.10: Plot of counts from four detectors with the theoretical probabilities, without the quarter-wave plate in setup. The differences in amplitude are due to the efficiencies of the detectors.

4.6. Calibration and Determination of Instrument Matrix

As explained earlier in §3.1.1., the output intensity (measured by the detectors) vector $\boldsymbol{I}$ can be linearly related to the input Stokes vector $\boldsymbol{S}$ by

$$\boldsymbol{I} = \boldsymbol{BS}\ , \tag{4.38}$$

where $\boldsymbol{B}$ is a 4 × 4 real matrix that is characteristic of the polarimeter at a given wavelength. With $\boldsymbol{B}$ known, the Stokes vector of an unknown input source can be easily established by measuring $\boldsymbol{I}$ and performing the matrix multiplication:

$$\boldsymbol{S} = \boldsymbol{B}^{-1}\boldsymbol{I}\ . \tag{4.39}$$

Hence, our next step will be to determine the instrument matrix $\boldsymbol{B}$.

Rewriting eq. (4.38) in an explicit form, we have

$$\begin{pmatrix} I_1 \\ I_2 \\ I_3 \\ I_4 \end{pmatrix} = \begin{pmatrix} b_{11} & b_{12} & b_{13} & b_{14} \\ b_{21} & b_{22} & b_{23} & b_{24} \\ b_{31} & b_{32} & b_{33} & b_{34} \\ b_{41} & b_{42} & b_{43} & b_{44} \end{pmatrix} \begin{pmatrix} S_0 \\ S_1 \\ S_2 \\ S_3 \end{pmatrix} . \tag{4.40}$$

From the above expression, we see that the elements of matrix $\boldsymbol{B}$ can be established experimentally by calibration. If we send in light of known polarisation states (i.e. the Stokes vector of input states are known), and note the intensities registered by the detectors (vector $\boldsymbol{I}$ is the normalised intensities measured by the four detectors), the elements of $\boldsymbol{B}$ can be calculated by solving a set of linear equations simultaneously.

To be more explicit, four different input states are prepared, sent into the polarimeter, and the intensities measured are taken down. Thus, we will have four sets of vectors $\boldsymbol{I}$ and $\boldsymbol{S}$. Each row of matrix $\boldsymbol{B}$ with four unknown can then be obtained from the four sets of equations constructed using the corresponding $\boldsymbol{I}$ and $\boldsymbol{S}$ elements.

4.6.1. Stokes Vector of Prepared Input States

We prepare the input states by placing a polariser, a half-wave plate and a quarter-wave plate in front of the polarimeter setup, as shown in Figure 4.7. Recall that from the previous section that the polarisation of light exiting the polariser wave-plates is

$$\left|\mathrm{prep}\right\rangle \equiv \mathbf{R}_{\mathrm{QWP}} \cdot \mathbf{R}_{\mathrm{HWP}} \cdot \begin{pmatrix} 1 \\ 0 \end{pmatrix} , \tag{4.41}$$

where $\left|\mathrm{prep}\right\rangle$ denotes the polarisation state prepared by us,

$$\mathbf{R}_{\mathrm{HWP}} = \begin{pmatrix} \cos 2\theta & -\sin 2\theta \\ -\sin 2\theta & -\cos 2\theta \end{pmatrix} , \tag{4.42}$$

$$\mathbf{R}_{\mathrm{QWP}} = \begin{pmatrix} \cos^2 \varphi + i \sin^2 \varphi & (-1+i)\sin\varphi\cos\varphi \\ (-1+i)\sin\varphi\cos\varphi & \sin^2\varphi + i\cos^2\varphi \end{pmatrix} , \tag{4.43}$$

and $\begin{pmatrix} 1 \\ 0 \end{pmatrix}$ is the horizontally polarised light after the beam passes through the polariser.

From eq. (2.3), we know that the density matrix of the input states is

$$\begin{aligned} \hat{\rho} &= \frac{1}{2}\sum_{i=0}^{3} s_i \cdot \hat{\sigma}_i \\ &= \frac{1}{2}\begin{pmatrix} 1+s_1 & s_2 - is_3 \\ s_2 + is_3 & 1 - s_1 \end{pmatrix} . \end{aligned} \tag{4.44}$$

However,

$$\begin{aligned} \hat{\rho} &= \left|\mathrm{prep}\right\rangle\left\langle\mathrm{prep}\right| \\ &= \frac{1}{2}\begin{pmatrix} 1+\cos(2\varphi)\cos(4\theta-2\varphi) & \sin(-2\varphi)\cos(4\theta-2\varphi) + i\sin(4\theta-2\varphi) \\ \sin(-2\varphi)\cos(4\theta-2\varphi) - i\sin(4\theta-2\varphi) & 1-\cos(2\varphi)\cos(4\theta-2\varphi) \end{pmatrix} \end{aligned} \tag{4.45}$$

By comparing the terms of eqs. (4.44) and (4.45), we arrived at

$$s_1 = \cos(2\varphi)\cos(4\theta - 2\varphi) , \tag{4.46a}$$

$$s_2 = -\sin(2\varphi)\cos(4\theta - 2\varphi) , \tag{4.46b}$$

$$s_3 = -\sin(4\theta - 2\varphi) \ , \tag{4.46c}$$

keeping in mind that θ and φ are the angles of the half-wave plate and quarter-wave plate respectively, not the angles of the spherical coordinate system. The term s_0 is of course just 1, since the Stokes vector is normalised.

4.6.2. Calibration with Imperfect Optical Elements

While we can easily determine the 16 elements of instrument matrix $\boldsymbol{B}$ from four prepared states, there is an alternative method which promises to reduce the errors of the matrix elements. It is an experimental reality that waveplates have some degree of wedge. In other words, the two surfaces of the waveplates are not perfectly parallel. This leads to two problems which we must confront: (i) the change in the phase retardance of the waveplates will not be the perfect π/2 for half-wave plate and π/4 for quarter-wave plate. As a result, our prepared states will not be exactly the states we are expecting. (ii) The direction of the beam will be slightly deflected as the waveplates are being rotated. This can have the effect of changing the detectors efficiencies, which in turn affect the values of the Stokes parameters computed from the detectors reading.

In order to minimise the errors contributed by the imperfections of the waveplates in general, we follow the calibration method proposed by Azzam *et al.* [22]. Instead of using a polariser, half-wave plate and quarter wave plate to prepare the input states, we remove the half-wave plate and use the polariser to set the degree of linear polarisation. As for the quarter-wave plate, we want to determine as much of our matrix elements as possible without using it.

Writing matrix $\boldsymbol{B}$ in terms of its columns, we have

$$\boldsymbol{B} = [\boldsymbol{B}_1 \ \ \boldsymbol{B}_2 \ \ \boldsymbol{B}_3 \ \ \boldsymbol{B}_4] \ . \tag{4.47}$$

The Stokes vector of incident linearly polarised light is given [22] by

$$\boldsymbol{S}_{LP} = [1 \;\; \cos 2\alpha \;\; \sin 2\alpha \;\; 0]^{\mathrm{T}} , \tag{4.48}$$

where the subscript LP denotes linear polarisation, the superscript T stands for transpose. The angle 2α is the spherical coordinates of the polarisation state in the three-dimensional space (recall that linearly polarised light lies on the equator), as shown in Figure 4.11. The factor of 2 in front is to account for the fact that any linear polarisation states is indistinguishable from one rotated by 180°.

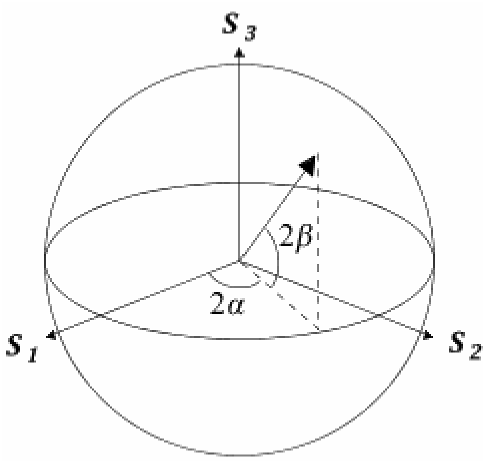

Figure 4.11: Stokes vector in terms of spherical coordinates. The 2 in front of α is to account for the fact that any linear polarisation state is indistinguishable from one rotated by 180°.

Substituting eqs. (4.48) and (4.47) into (4.38), we observe that

$$\boldsymbol{I}_{LP} = \boldsymbol{B}_1 + \boldsymbol{B}_2 \cos 2\alpha + \boldsymbol{B}_3 \sin 2\alpha \, . \tag{4.49}$$

The above equation implies that the first three columns of the matrix $\boldsymbol{B}$ can be obtained without the quarter-wave plate (since it is responsible for introducing circular polarisation to the light). By rotating the polariser through an angle and collecting the readings for each of the detectors, we can fit the set of data to the eq. (4.49) to obtain the values of the elements in the first three columns of the instrument matrix. To put it in another way, the intensity readings for a detector – let's call it detector i – are plotted out over the angle range. It is then fitted to the expression

$$f(\alpha) = b_{i1} + b_{i2} \cos 2\alpha + b_{i3} \sin 2\alpha \, , \tag{4.50}$$

to obtain the values of b_{i1}, b_{i2} and b_{i3}, which are the first three matrix elements of row i. Here, α is the angle of the polariser. The figures below show our results:

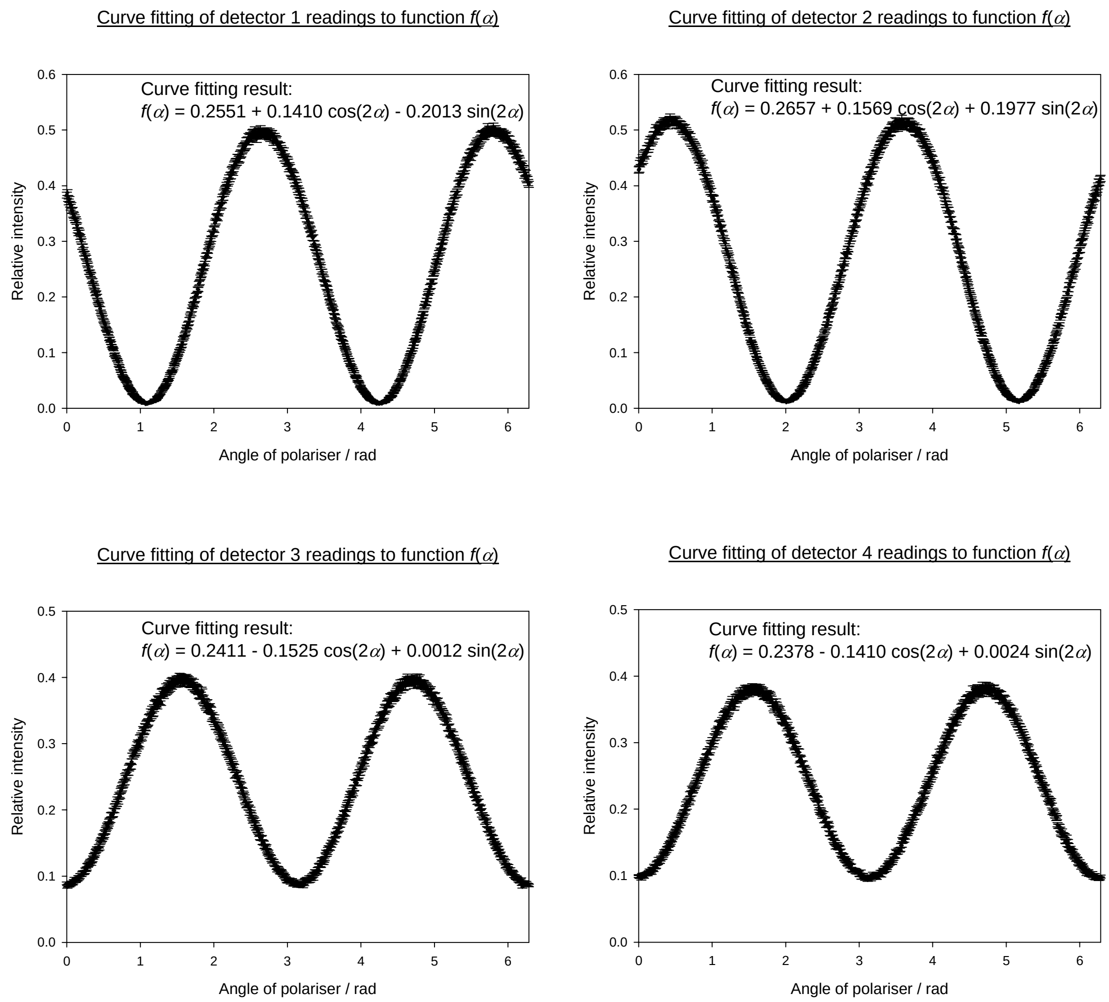

Figure 4.12: From top left and right, to bottom left and right: curve fitting of readings from detector 1, 2, 3, and 4 to eq. (4.54). The values obtained for the variables b*i*1, b*i*2 and b*i*3 form the *i*-th row of the instrument matrix.

We obtain:

$$\mathbf{B} = \begin{pmatrix} 0.2551 & 0.1410 & -0.2013 & b_{14} \\ 0.2657 & 0.1569 & 0.1977 & b_{24} \\ 0.2411 & -0.1525 & 0.0012 & b_{34} \\ 0.2378 & -0.1410 & 0.0024 & b_{44} \end{pmatrix}. \tag{4.51}$$

The last column of matrix $\boldsymbol{B}$ is dependent on circularly polarised light, which has the Stokes vector

$$\boldsymbol{S}_{CP} = [1 \quad 0 \quad 0 \quad \pm 1]^{\mathrm{T}} , \tag{4.52}$$

where the subscript *CP* refers to circular polarisation, and the + and – sign apply to right- (RCP) and left- handed (LCP) polarisation respectively. Substituting eqs. (4.52) and (4.47) into (4.38) gives

$$\boldsymbol{I}_{RCP} = \boldsymbol{B}_1 + \boldsymbol{B}_4 , \tag{4.53}$$

$$\boldsymbol{I}_{LCP} = \boldsymbol{B}_1 - \boldsymbol{B}_4 , \tag{4.54}$$

where the intensity vector $\boldsymbol{I}$ has been normalised with respect to the total counts. The two equations above can be combined to give

$$\boldsymbol{B}_4 = \tfrac{1}{2} (\boldsymbol{I}_{RCP} - \boldsymbol{I}_{LCP}) , \tag{4.55}$$

As we pointed out earlier, the imperfection of the quarter-wave plate will not allow us to generate the exact RCP and LCP state. The idea behind the method by Azzam *et al.* is this: instead of generating the exact RCP state (which is the north pole on the Poincaré sphere), the state generated will be slightly displaced. If we now rotate the polariser and the quarter-wave plate by 90°, the state which we generate will be exactly on the other side of the north pole, as shown in Figure 4.13 below.

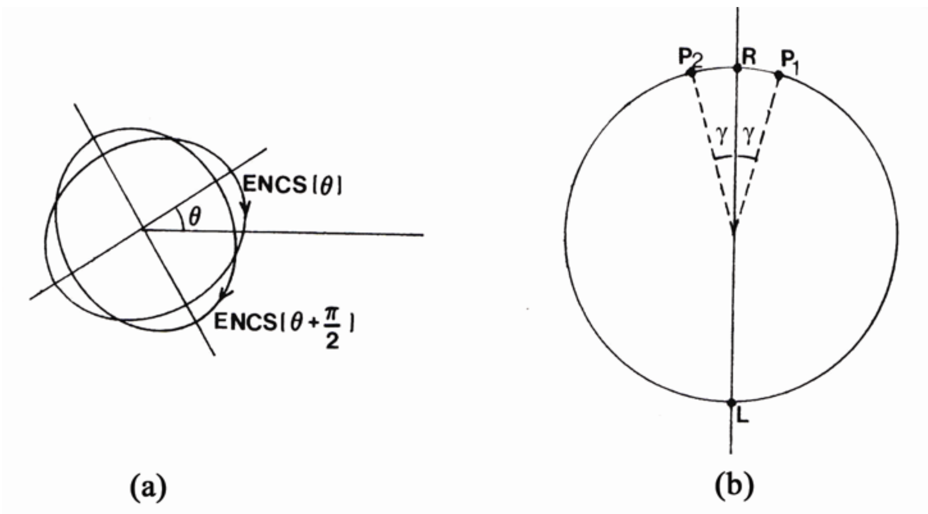

Figure 4.13(a): Instead of generating the exact circular RCP and LCP states, what we have instead is an elliptical-near-circular state (ENCS). By rotating it by 90° and averaging it with the former state, we will obtain a circular state. **(b):** Cross section of the Poincaré sphere. The two ENCS states of part (a) are actually located directly opposite each other on the sphere. Picture adapted from [22].

To obtain the desired data for a RCP state, we simply average the results we have for these two states. The same argument applies to the LCP state, which lies on the south pole of the Poincaré sphere. We have

Polarisation States	Apparent RCP	Apparent RCP + 90°	Apparent LCP	Apparent LCP + 90°
Waveplate Setting	Polariser: 45° QWP : 0°	Polariser: 135° QWP : 90°	Polariser: -45° QWP : 0°	Polariser: 45° QWP : 90°
Detector 1	220 747	261 852	379 397	365 474
Detector 2	393 410	387 999	221 437	261 795
Detector 3	95 611	87 128	467 039	481 565
Detector 4	518 321	517 274	116 323	115 207
Total counts	1 228 089	1 254 253	1 184 196	1 224 341

Table 4.1: Photon counts of the apparent RCP and LCP states, with their counterparts that are rotated by 90°. Their respective waveplate settings are given as well. They are used to compute the last column of the instrument matrix.

After normalising the counts for each column, we get

$$I_{RCP'} = \begin{pmatrix} 0.1797 \\ 0.3203 \\ 0.0779 \\ 0.4221 \end{pmatrix}, \; I_{RCP'+90^o} = \begin{pmatrix} 0.2088 \\ 0.3093 \\ 0.0695 \\ 0.4124 \end{pmatrix}, \; I_{LCP'} = \begin{pmatrix} 0.3204 \\ 0.1870 \\ 0.3944 \\ 0.0982 \end{pmatrix}, \; I_{LCP'+90^o} = \begin{pmatrix} 0.2985 \\ 0.2138 \\ 0.3936 \\ 0.0941 \end{pmatrix} \quad (4.56)$$

where the prime which accompanies the polarisation states denotes that state is the apparent one instead of the exact state.

Averaging the results of eq. (4.56) give

$$I_{RCP} = \frac{\left(I_{RCP'} + I_{RCP'+90^o}\right)}{2} = \begin{pmatrix} 0.1943 \\ 0.3148 \\ 0.0737 \\ 0.4172 \end{pmatrix}, \tag{4.57}$$

$$I_{LCP} = \frac{\left(I_{LCP'} + I_{LCP'+90^o}\right)}{2} = \begin{pmatrix} 0.3094 \\ 0.2004 \\ 0.3940 \\ 0.0962 \end{pmatrix}. \tag{4.58}$$

By perform eq. (4.55), we obtain the final column of matrix ***B***. Thus, the complete instrument matrix is

$$\mathbf{B} = \begin{pmatrix} 0.2551 & 0.1410 & -0.2013 & -0.0576 \\ 0.2657 & 0.1569 & 0.1977 & 0.0572 \\ 0.2411 & -0.1525 & 0.0012 & -0.1602 \\ 0.2378 & -0.1410 & 0.0024 & 0.1605 \end{pmatrix}, \tag{4.59}$$

while

$$\mathbf{B}^{-1} = \begin{pmatrix} 0.9933 & 0.9930 & 1.008 & 1.008 \\ 1.589 & 1.650 & -1.755 & -1.769 \\ -2.585 & 2.431 & 0.9202 & -0.8756 \\ -0.03708 & -0.05805 & -3.048 & 3.195 \end{pmatrix}. \tag{4.60}$$

CHAPTER 5

Performing Tomographic Measurement

5.1. Single-Qubit System

Armed with the instrument matrix $\boldsymbol{B}^{-1}$, we can now translate the detector counts for any polarisation states into its corresponding Stokes vector. To gauge how accurate our polarimeter is in determining the polarisation states, we attempt to map out the polarisation states of the whole Poincaré sphere using the setup shown in Figure 4.6.

The polariser and the quarter-wave plate are attached to a motor each, which are in turn connected to the computer. We take the quarter-wave plate through an angle of 180^o. For every degree of the quarter-wave plate, the half-wave plate is rotated through a complete revolution of 360^o, pausing at every 2^o to collect the photon counts for 20 seconds. Thus, a set of data is collected over the whole surface of the Poincaré sphere.

5.1.1. Results

With this set of data, the Stokes vectors of the prepared states can be computed from eq. (4.46), using the angles of the half-wave plate and quarter-wave plate. On the other hand, the Stokes vectors are reconstructed from the detectors counts using eq. (4.39).

To characterise the accuracy of our results, we compute the Uhlmann fidelity[11], F, defined by

$$F = \left(\mathrm{Tr}\left\{ \sqrt{\sqrt{\rho_{prep}}\,\rho_{recon}\sqrt{\rho_{prep}}} \right\} \right)^2 , \tag{5.1}$$

where ρ_{prep} and ρ_{recon} are the density matrices of the prepared and the reconstructed states respectively. For pure states, eq. (5.1) reduces [23] to

$$F = \mathrm{Tr}\left\{ \rho_{prep} \cdot \rho_{recon} \right\} . \tag{5.2}$$

which further simplifies to

$$F = \frac{1}{2}\left(\vec{S}_{prep} \cdot \vec{S}_{recon} \right) , \tag{5.3}$$

for the single-qubit case. In eq. (5.3), $\vec{S}_{prep}$ and $\vec{S}_{recon}$ are the normalised prepared and reconstructed Stokes vectors. Essentially, eq. (5.3) gives us the projection of the $\vec{S}_{recon}$ onto $\vec{S}_{prep}$, with 1 being a perfect match.

Since the surface of the Poincaré sphere is two-dimensional, we compute the fidelity for all the corresponding Stokes vector and project it onto a flat surface with the longitudes and latitude as the coordinates. Recall from chapter one that the reduced Stokes vector is simply the Cartesian coordinates of a point in a three-dimensional Poincaré sphere. Hence, the longitude and the latitude are given as

$$\text{Longitude} = \cos^{-1} s_1 = \sin^{-1} s_2 \tag{5.4}$$

$$\text{Latitude} = \sin^{-1} s_3 \tag{5.5}$$

The Stokes parameters s_1, s_2, s_3 used in eqs. (5.4) and (5.5) are of course those of the prepared Stokes vectors, since they are what we prepared in theory.

[11] We note that some groups use an alternative convention for fidelity, that is equal to the square root of the formula given by eq. (5.1).

The results are shown below in Figure 5.1 and we observed a minimum fidelity of 0.994.

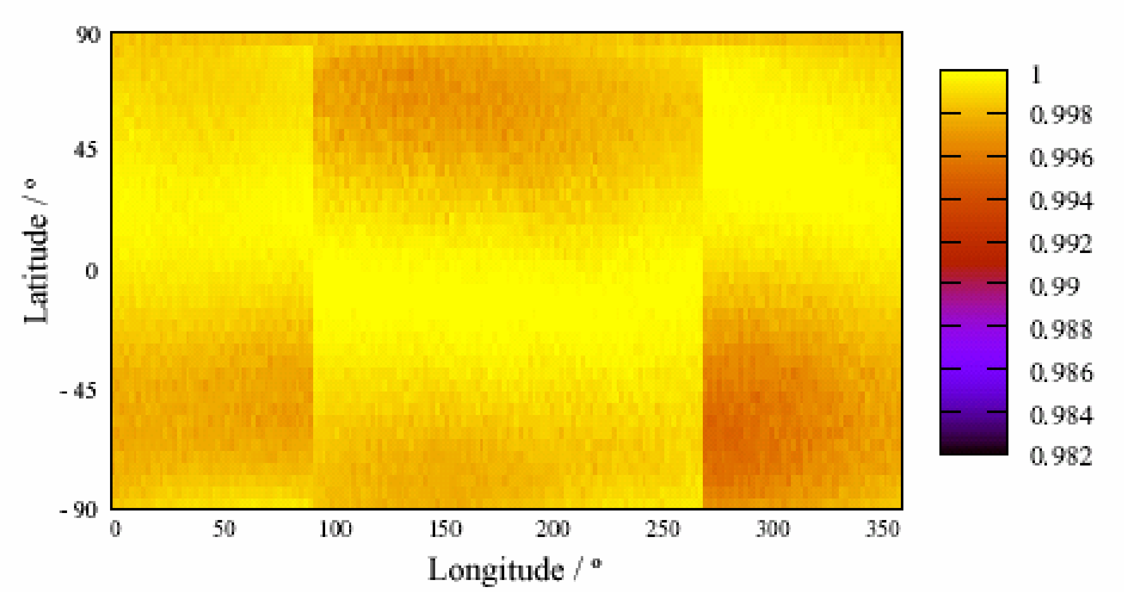

Figure 5.1: A plot of the fidelity of the estimated states to the prepared states over the whole Poincaré sphere. The minimum fidelity achieved is 0.994.

In general, we observe that a central belt in the region of the equator has a slightly higher fidelity than surrounding region. This is hardly surprising, once we remember that in the calibration and determination of the instrument matrix, we use linearly polarised states (which fall on the equator of the Poincaré sphere) and the right- and left- circular states. Hence, we would expect these polarisation states to give us a more accurate match of $\vec{S}_{recon}$ onto $\vec{S}_{prep}$.

5.1.2. Error Analysis

One source of error for this experiment is the error of counting statistics. The number of photons generated from a SPDC process has a Poissonian distribution [24]. Hence, without even taking into account the efficiencies of the detectors, the photon counts have the characteristic Poissonian variance that is equal to itself.

However, this error can easily be reduced by taking each measurement on a larger ensemble. By taking the photon counts over a 20 seconds interval, the minimum number of counts we get is around 6000, which give us an uncertainty of $\sqrt{6000} = \pm 77$ photons or ±1%.

We perform a simple error propagation to see the expected error of our instrument matrix as well as the reconstructed Stokes vector.

For the first three columns of the instrument matrix, we have the uncertainty from the curve fitting of the data to the curve of eq. (4.50).

$$\mathbf{B} = \begin{pmatrix} 0.2551 \pm 0.0002 & 0.1410 \pm 0.0002 & -0.2013 \pm 0.0002 & b_{14} \\ 0.2657 \pm 0.0002 & 0.1569 \pm 0.0002 & 0.1977 \pm 0.0002 & b_{24} \\ 0.2411 \pm 0.0001 & -0.1525 \pm 0.0001 & 0.0012 \pm 0.0001 & b_{34} \\ 0.2378 \pm 0.0001 & -0.1410 \pm 0.0002 & 0.0024 \pm 0.0002 & b_{44} \end{pmatrix}. \tag{5.6}$$

The intensity vectors of eq. (4.56) are computed by dividing the counts of each column of Table 4.1 by its respective total count, i.e. $I_j = N_j \,/\, N_{Total}$. Hence, the variance of I_j is given by

$$\begin{aligned} {\sigma_{I_j}}^2 &= {\sigma_{N_j}}^2 \left(\frac{\partial I_j}{\partial N_j} \right)^2 + {\sigma_{N_{Total}}}^2 \left(\frac{\partial I_j}{\partial N_{Total}} \right)^2 \\ &= \frac{{\sigma_{N_j}}^2 {N_{Total}}^2 + {\sigma_{N_{Total}}}^2 {N_j}^2}{{N_{Total}}^4}, \end{aligned} \tag{5.7}$$

where σ_{N_j} is simply $\sqrt{N_j}$. And we have

$$I_{RCP'} = \begin{pmatrix} 0.1797 \pm 0.0004 \\ 0.3203 \pm 0.0006 \\ 0.0779 \pm 0.0003 \\ 0.4221 \pm 0.0007 \end{pmatrix}, \quad I_{RCP'+90^o} = \begin{pmatrix} 0.2088 \pm 0.0004 \\ 0.3093 \pm 0.0006 \\ 0.0695 \pm 0.0002 \\ 0.4124 \pm 0.0007 \end{pmatrix},$$

$$I_{LCP'} = \begin{pmatrix} 0.3204 \pm 0.0006 \\ 0.1870 \pm 0.0004 \\ 0.3944 \pm 0.0007 \\ 0.0982 \pm 0.0003 \end{pmatrix}, \quad I_{LCP'+90^o} = \begin{pmatrix} 0.2985 \pm 0.0006 \\ 0.2138 \pm 0.0005 \\ 0.3936 \pm 0.0007 \\ 0.0941 \pm 0.0003 \end{pmatrix}. \tag{5.8}$$

Therefore, our instrument matrix and its inverse have the errors

$$\mathbf{B} = \begin{pmatrix} 0.2551 \pm 0.0002 & 0.1410 \pm 0.0002 & -0.2013 \pm 0.0002 & -0.0576 \pm 0.0005 \\ 0.2657 \pm 0.0002 & 0.1569 \pm 0.0002 & 0.1977 \pm 0.0002 & 0.0572 \pm 0.0006 \\ 0.2411 \pm 0.0001 & -0.1525 \pm 0.0001 & 0.0012 \pm 0.0001 & -0.1602 \pm 0.0005 \\ 0.2378 \pm 0.0001 & -0.1410 \pm 0.0002 & 0.0024 \pm 0.0002 & 0.1605 \pm 0.0005 \end{pmatrix}$$

(5.9)

$$\mathbf{B}^{-1} = \begin{pmatrix} 0.9933 \pm 0.0002 & 0.993 \pm 0.003 & 1.008 \pm 0.006 & 1.008 \pm 0.005 \\ 1.5890 \pm 0.0002 & 1.6501 \pm 0.0008 & -1.7547 \pm 0.0001 & -1.7692 \pm 0.0001 \\ -2.5853 \pm 0.0001 & 2.4308 \pm 0.0005 & 0.9202 \pm 0.0005 & -0.8756 \pm 0.0009 \\ -0.0371 \pm 0.0003 & -0.058 \pm 0.001 & -3.0483 \pm 0.0003 & 3.1953 \pm 0.0008 \end{pmatrix}$$

(5.10)

From our plot of fidelity, we pick the point with latitude of -58.5^o and longitude of 282^o, which has a relatively low fidelity of 0.994, and compute the uncertainty of its normalised intensity vector:

$$\mathbf{I} = \begin{pmatrix} 0.478 \pm 0.002 \\ 0.1208 \pm 0.0008 \\ 0.328 \pm 0.002 \\ 0.0735 \pm 0.0006 \end{pmatrix}. \tag{5.11}$$

This gives us an uncertainty of ±0.005 for the fidelity of this particular state. Hence, our minimum fidelity is 99.4±0.5 %.

5.2. Pair-Qubit System

5.2.1. Setup, Electronics, and Data Collection

In order to construct the density matrix for an entangled photon pair, we need to detect photon pairs that are correlated. For this purpose, another polarimeter similar to the one we have discussed in the last chapter is built. The entangled photon pairs generated from SPDC are sent separately into two optical fibres, which are in turn connected to the two polarimeters.

We are interested to count the entangled photon pairs, and not just any photon that arrives at the detectors. In other words, whether we decide to count a photon that is registered in a detector depends on the condition of whether another photon is registered in one of the detectors of the other polarimeter at approximately the same instance. This conditional counting of photon pairs can be accomplished with an electronic circuit of *AND* gates and delay lines, combined with a computer program to set the time window for coincidence count.[12] The computer program tells the computer to consider a pair of photons as correlated only if they are detected within the time window. In our experiment, the time window is set to be 6 ns.

Since our two polarimeters have four detectors each, there are sixteen possible coincidences between the detectors of the two polarimeters. A measurement of these sixteen coincidence possibilities is what we need to determine the sixteen elements of the probability density matrix of entangled photon pairs.

5.2.2. Accidental Coincidences

Just as the dark counts need to be corrected for in single-qubit experiments, we need to take into account the accidental coincidences in pair-qubits experiment. Due to the fact that several pairs of photons are being generated at the same time, two uncorrelated photons might be detected as coincidence. This is the phenomenon which we call accidental coincidence, and like the dark counts, they tend to raise all measured counts, thus giving a false impression of the actual ratio of the coincidence counts.

[12] I would like to mention that credits for setting up the electronic circuits and writing the program to count the coincidences go solely to Alexander Ling. I did not participate in this part of the project.

These accidental coincidences can be modelled by considering the probability for a detector to register a count during the time window of the coincidences [9]. Let S_p and S_q by the number counts registered separately by detectors p and q in the duration of t. Then, accidental coincidence between detector p and q, over a time period of t', can be approximated as

$$c_{p,q}^{\text{accid}} \approx \frac{S_p S_q \Delta\tau}{t} t' \ , \tag{5.12}$$

where $\Delta\tau$ is the coincidence time window.

Before any measurement of the coincidence count, we first measure photon counts in all the eight detectors. The accidental coincidence is the computed and subtracted from subsequent coincidence measurement. For ease in calculation, we chose $t = t'$ so that eq. (5.12) reduces to

$$c_{p,q}^{\text{accid}} \approx S_p S_q \Delta\tau \ . \tag{5.13}$$

We do not need to consider the dark counts in two-qubits experiments because they will not be registered by the counter program unless they are detected within the coincidence time frame, and the accidental coincidences for dark counts are extremely small.

5.2.3. Results

The SPDC source is used to generate the Bell state

$$\begin{aligned} \left|\Psi^{\pm}\right\rangle &= \frac{1}{\sqrt{2}}\left(\left|HV\right\rangle \pm \left|VH\right\rangle\right), \\ \left|\Phi^{\pm}\right\rangle &= \frac{1}{\sqrt{2}}\left(\left|HH\right\rangle \pm \left|VV\right\rangle\right). \end{aligned} \tag{5.14}$$

For the singlet state $\left|\Psi^{-}\right\rangle$,

$$\begin{aligned}
\left|\Psi^{-}\right\rangle &= \frac{1}{\sqrt{2}}\left(\left|HV\right\rangle - \left|VH\right\rangle\right) \\
&= \frac{1}{\sqrt{2}}\left(\left|H\right\rangle \otimes \left|V\right\rangle + \left|V\right\rangle \otimes \left|H\right\rangle\right) \\
&= \frac{1}{\sqrt{2}}\left[\begin{pmatrix}1\\0\end{pmatrix} \otimes \begin{pmatrix}0\\1\end{pmatrix} - \begin{pmatrix}0\\1\end{pmatrix} \otimes \begin{pmatrix}1\\0\end{pmatrix}\right] \\
&= \frac{1}{\sqrt{2}}\begin{pmatrix}0\\1\\-1\\0\end{pmatrix},
\end{aligned} \tag{5.15}$$

which has the density matrix

$$\left|\Psi^{-}\right\rangle\left\langle\Psi^{-}\right| = \frac{1}{2}\begin{pmatrix}0 & 0 & 0 & 0\\ 0 & 1 & -1 & 0\\ 0 & -1 & 1 & 0\\ 0 & 0 & 0 & 0\end{pmatrix}. \tag{5.16}$$

Similarly,

$$\left|\Psi^{+}\right\rangle\left\langle\Psi^{+}\right| = \frac{1}{2}\begin{pmatrix}0 & 0 & 0 & 0\\ 0 & 1 & 1 & 0\\ 0 & 1 & 1 & 0\\ 0 & 0 & 0 & 0\end{pmatrix}, \tag{5.17}$$

$$\left|\Phi^{-}\right\rangle\left\langle\Phi^{-}\right| = \frac{1}{2}\begin{pmatrix}1 & 0 & 0 & -1\\ 0 & 0 & 0 & 0\\ 0 & 0 & 0 & 0\\ -1 & 0 & 0 & 1\end{pmatrix}, \tag{5.18}$$

$$\left|\Phi^{+}\right\rangle\left\langle\Phi^{+}\right| = \frac{1}{2}\begin{pmatrix}1 & 0 & 0 & 1\\ 0 & 0 & 0 & 0\\ 0 & 0 & 0 & 0\\ 1 & 0 & 0 & 1\end{pmatrix}. \tag{5.19}$$

Repeating the same procedure outlined previously, we obtain the instrument matrices, **A** and **B**, for the two polarimeters.

$$\mathbf{A} = \begin{pmatrix} 0.961 & 0.611 & 0.736 & 0.024 \\ 0.935 & 0.584 & -0.726 & -0.027 \\ 1.067 & -0.615 & 0.005 & -0.799 \\ 1.034 & -0.555 & -0.024 & 0.843 \end{pmatrix}, \tag{5.20}$$

$$\mathbf{B} = \begin{pmatrix} 1.039 & 0.650 & 0.779 & 0.053 \\ 1.065 & 0.520 & -0.861 & -0.053 \\ 0.974 & -0.619 & -0.041 & -0.799 \\ 0.925 & -0.559 & 0.064 & 0.820 \end{pmatrix}. \tag{5.21}$$

Since the rows of the instrument matrices can be seen as the Stokes vectors of the calibration states, which in our case are the tetrahedron vectors, we can construct the POVMs for the two polarimeters, as given by eq. (2.16):

$$\hat{A}_j = \frac{1}{4}\sum_{k=0}^{3} a_{jk}\hat{\sigma}_k \quad , \quad j = 1, 2, 3, 4, \tag{5.22}$$

where a_{jk} is the j^{th} row and k^{th} column of the instrument matrix **A** (we choose to let k range from 0 to 3 instead of 1 to 4 so that the indices will match with those of the Pauli operators). Similarly, we have

$$\hat{B}_j = \frac{1}{4}\sum_{k=0}^{3} b_{jk}\hat{\sigma}_k \quad , \quad j = 1, 2, 3, 4, \tag{5.23}$$

for polarimeter 2.

For the singlet state, our coincidences vector is

$$C_{\Psi-} = (628, 13281, 20626, 19435, 17525, 965, 17664, 18643, 16669, 13776, 496, 13524, 11288, 16126, 17041, 415)^{T}, \tag{5.24}$$

where its terms correspond to the coincidence counts between the two polarimeters, shown in Figure 5.2.

We can now proceed to compute the density matrix for the singlet state $\left|\Psi^{-}\right\rangle$, by following the steps discussed in chapter 2. First, we need to calculate the 16 $\hat{\Gamma}$ matrices, each of which is the tensor product of two Pauli operators, as given in eq. (2.21). Next,

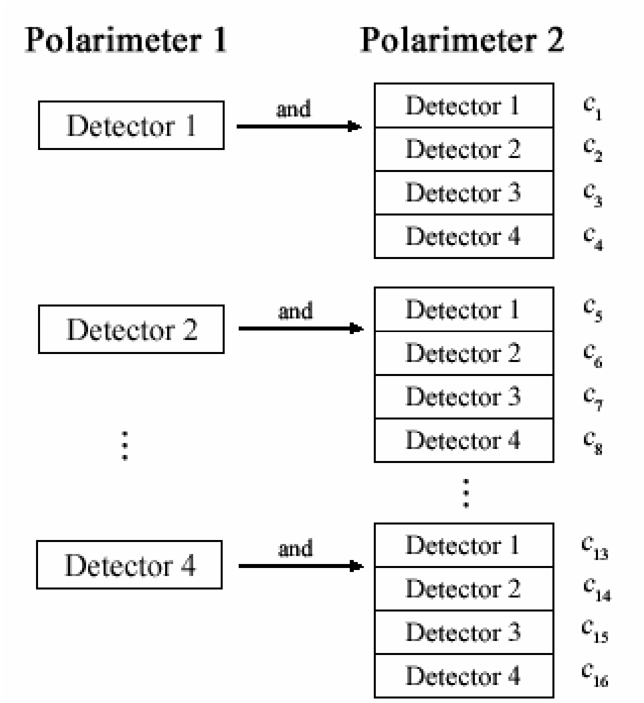

Figure 5.2: A scheme showing the correlation in question for each component of the coincidence vector.

we construct the 16 × 16 matrix **W**, given in eq. (2.23). The 16 $\left|\psi_\mu\right\rangle\left\langle\psi_\mu\right|$ are the tensor product between the two POVMs:

$$\left|\psi_\mu\right\rangle\left\langle\psi_\mu\right| = \hat{A}_l \otimes \hat{B}_m \ , \quad l \text{ and } m = 1, 2, 3, 4. \tag{5.25}$$

Finally, we take the inverse of matrix **W** and compute the desired density matrix using eq. (2.25)

$$\hat{\rho} = \sum_{\nu=1}^{16}\sum_{\mu=1}^{16} \hat{\Gamma}_\nu \left(W^{-1}\right)_{\mu,\nu} C_\mu \ . \tag{5.26}$$

The real components of $\hat{\rho}$ are

$$\mathrm{Re}\left(\hat{\rho}_{\Psi_-}\right) = \begin{pmatrix} 0.003 & -0.021 & 0.026 & -0.018 \\ -0.021 & 0.464 & 0.469 & -0.027 \\ 0.026 & -0.469 & 0.540 & 0.019 \\ -0.018 & -0.027 & 0.019 & -0.006 \end{pmatrix}, \tag{5.27}$$

while its imaginary components have a maximum value of 0.05. Figure 5.3 shows a plot of the density matrix.

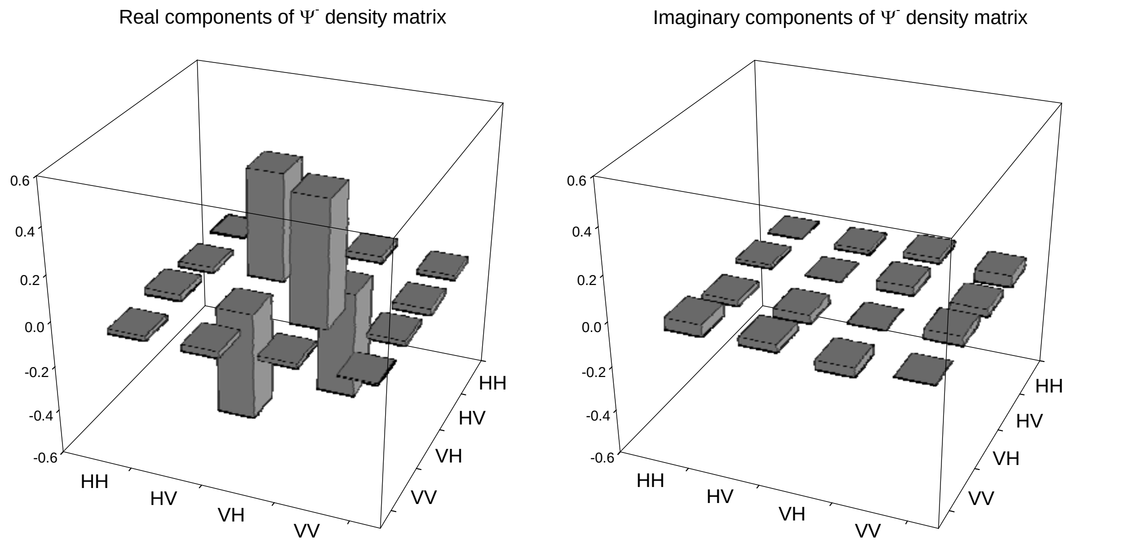

Figure 5.3: Graphical representation of the reconstructed density matrix of our Ψ^- state. The left plot shows the real part while the right plot shows the imaginary part.

The fidelity of our matrix to the ideal $\left|\Psi^-\right\rangle$ matrix is 0.971 computed using eq. (5.1).

We do the same for other Bell states and obtain

$$C_{\Psi+} = (13161, 1100, 20712, 20264, 807, 17923, 18846, 16204, 14460, 15767, 13211, 372, 16630, 11033, 885, 17474)^T, \tag{5.28}$$

$$C_{\Phi-} = (11819, 23881, 7307, 7941, 24552, 7123, 11806, 9463, 5496, 6702, 23987, 10584, 7314, 2885, 7501, 23286)^T, \tag{5.29}$$

$$C_{\Phi+} = (25143, 8525, 10478, 8844, 10425, 24302, 8396, 8626, 7356, 8910, 9099, 24592, 6262, 6353, 23614, 9483)^T, \tag{5.30}$$

And

$$\mathrm{Re}(\hat{\rho}_{\Psi+}) = \begin{pmatrix} 0.010 & -0.029 & -0.042 & 0.020 \\ -0.029 & 0.460 & 0.471 & -0.035 \\ -0.042 & 0.471 & 0.533 & 0.042 \\ 0.020 & -0.035 & 0.042 & -0.002 \end{pmatrix}, \tag{5.31}$$

$$\mathrm{Re}(\hat{\rho}_{\Phi-}) = \begin{pmatrix} 0.540 & 0.031 & 0.017 & -0.491 \\ 0.031 & -0.048 & -0.031 & 0.027 \\ 0.017 & -0.031 & -0.015 & -0.038 \\ -0.491 & 0.027 & -0.038 & 0.523 \end{pmatrix}, \tag{5.32}$$

$$\mathrm{Re}(\hat{\rho}_{\Phi+}) = \begin{pmatrix} 0.506 & -0.029 & 0.035 & 0.473 \\ -0.029 & 0.014 & 0.031 & -0.030 \\ 0.035 & 0.031 & -0.012 & 0.047 \\ 0.473 & -0.030 & 0.047 & -0.002 \end{pmatrix}, \tag{5.33}$$

Plots of these density matrices are given in Figure 5.4. The fidelity of $\hat{\rho}_{\Psi+}$, $\hat{\rho}_{\Phi-}$, and $\hat{\rho}_{\Phi+}$ to their ideal counterparts are 0.967, 1.023, 0.972.

5.2.4. Error Analysis

Adopting the same procedure as what we did for single-qubit system, we see that the errors of the two instrument matrices are

$$\mathbf{A} = \begin{pmatrix} 0.961 \pm 0.002 & 0.611 \pm 0.006 & 0.736 \pm 0.004 & 0.024 \pm 0.002 \\ 0.935 \pm 0.002 & 0.584 \pm 0.006 & -0.726 \pm 0.004 & -0.027 \pm 0.002 \\ 1.067 \pm 0.005 & -0.615 \pm 0.006 & 0.005 \pm 0.0006 & -0.799 \pm 0.009 \\ 1.034 \pm 0.003 & -0.555 \pm 0.004 & -0.024 \pm 0.0005 & 0.843 \pm 0.007 \end{pmatrix} \tag{5.39}$$

$$\mathbf{B} = \begin{pmatrix} 1.039 \pm 0.005 & 0.650 \pm 0.005 & 0.779 \pm 0.005 & 0.053 \pm 0.002 \\ 1.065 \pm 0.004 & 0.520 \pm 0.004 & -0.861 \pm 0.004 & -0.053 \pm 0.002 \\ 0.974 \pm 0.006 & -0.619 \pm 0.004 & -0.041 \pm 0.004 & -0.799 \pm 0.006 \\ 0.925 \pm 0.005 & -0.559 \pm 0.004 & 0.064 \pm 0.004 & 0.820 \pm 0.005 \end{pmatrix} \tag{5.40}$$

Bringing these errors forward, give the elements of our density matrix an error of order 0.001 to 0.003, while the uncertainty of our fidelity are: 97.1±0.4 %, 96.7±0.3 %, 102.3±0.3 %, 97.2±0.3 %.

The deviations of our density matrices from their ideal cases are reasonably small, though they are slightly larger than the propagated error from the curve fitting and the Poissonian statistical noise of the coherent states. Factors that contribute to the deviations can come from the setup equipments, such as the minute fluctuation in the intensity of the laser. While this is also a source of errors for the tomographic measurement of single-qubit state, it appears that measuring the coincidence counts might have place a stricter demand on the equipments to be near-perfect. However, one

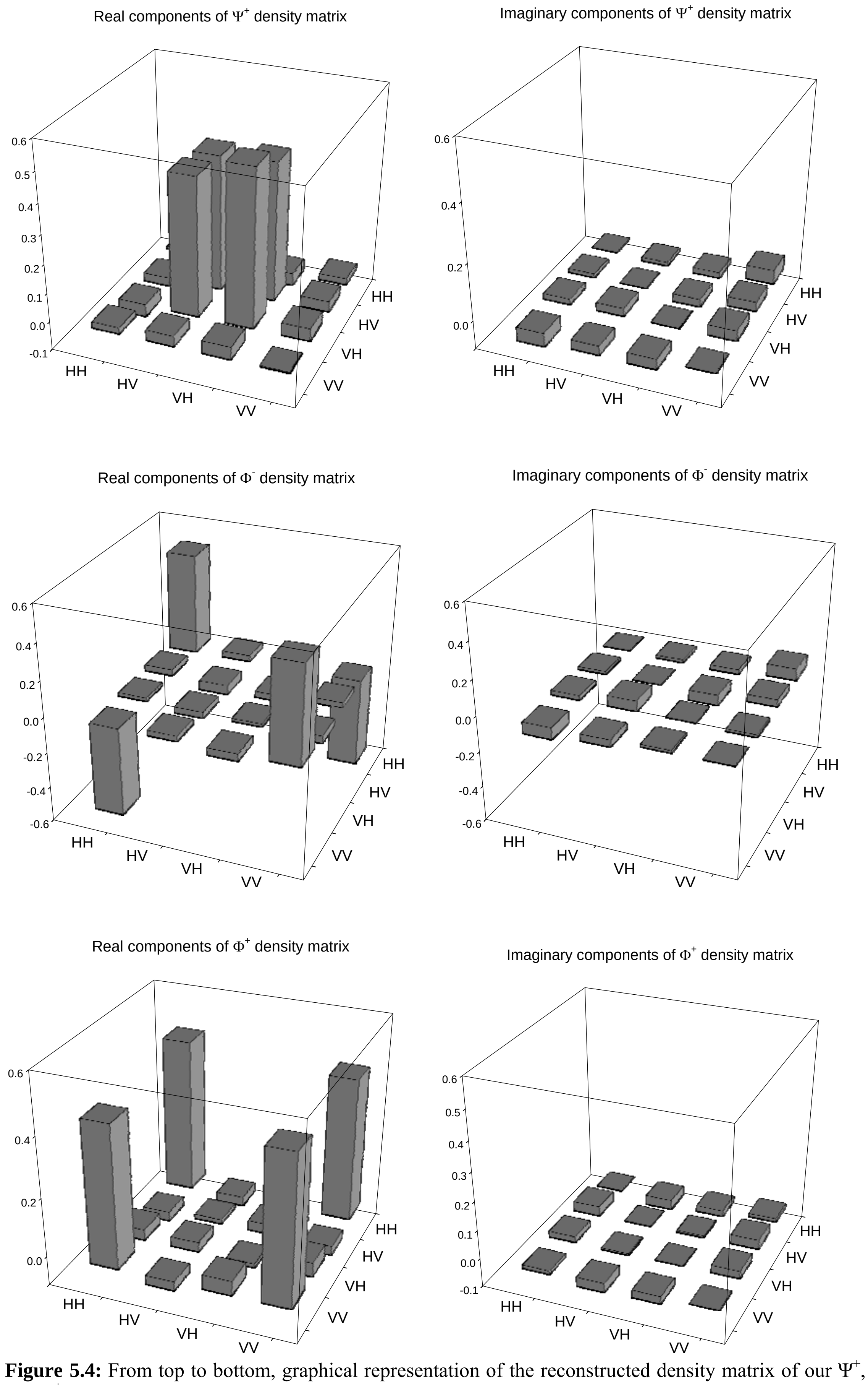

Figure 5.4: From top to bottom, graphical representation of the reconstructed density matrix of our Ψ^+, Φ^- , Φ^+ state. The left plots show the real parts while the right plots show the imaginary parts.

should be able to improve on the density matrix reconstructed from the measurements by fine-tuning the experimental setup and attempting to model the intensity drift of the laser.

We have followed the traditional method of error analysis, which involves propagating errors from their sources. We note in passing that James et al. [2] and Altepeter [9] have used statistical and numerical methods to predict the spread in the values of the derived quantities.

CHAPTER 6

Conclusion

We have given a detailed account of the procedure for assembling a polarimeter with no moving parts that is based on the tetrahedron POVM measurements. It is this very correspondence of the POVM to a set of regular tetrahedron vectors that makes our polarimeter optimal.

The experimental results on the state estimation of single- and two-qubit systems using this polarimeter, have shown a consistently high fidelity. For two-qubit systems, the reconstructed density matrix is relatively close to the ideal case, and one should be able to further improve it by fine tuning the setup and taking into account other sources of errors.

Our polarimeter is sensitive to low light intensity and hence will be helpful in many areas. In particular, we would like to point out that it can be used to realise a recently proposed protocol for key distribution in quantum cryptography [3, 4]. This protocol is based on minimal qubit tomography and it promises higher efficiency and noise tolerance, as compared to a 6-state protocol which also offers full state tomography.

Although our state tomography experiment was done on single- and two-qubit system, it can be extended to any number of qubits. Of course, the number of measurements needed to perform the tomography will grow exponentially with the number of qubits. This once again underscores the advantage of the minimal state tomography which we have implemented: only the minimal number of measurements that is required is taken.

Appendix

A. Pictures of Experimental Setup

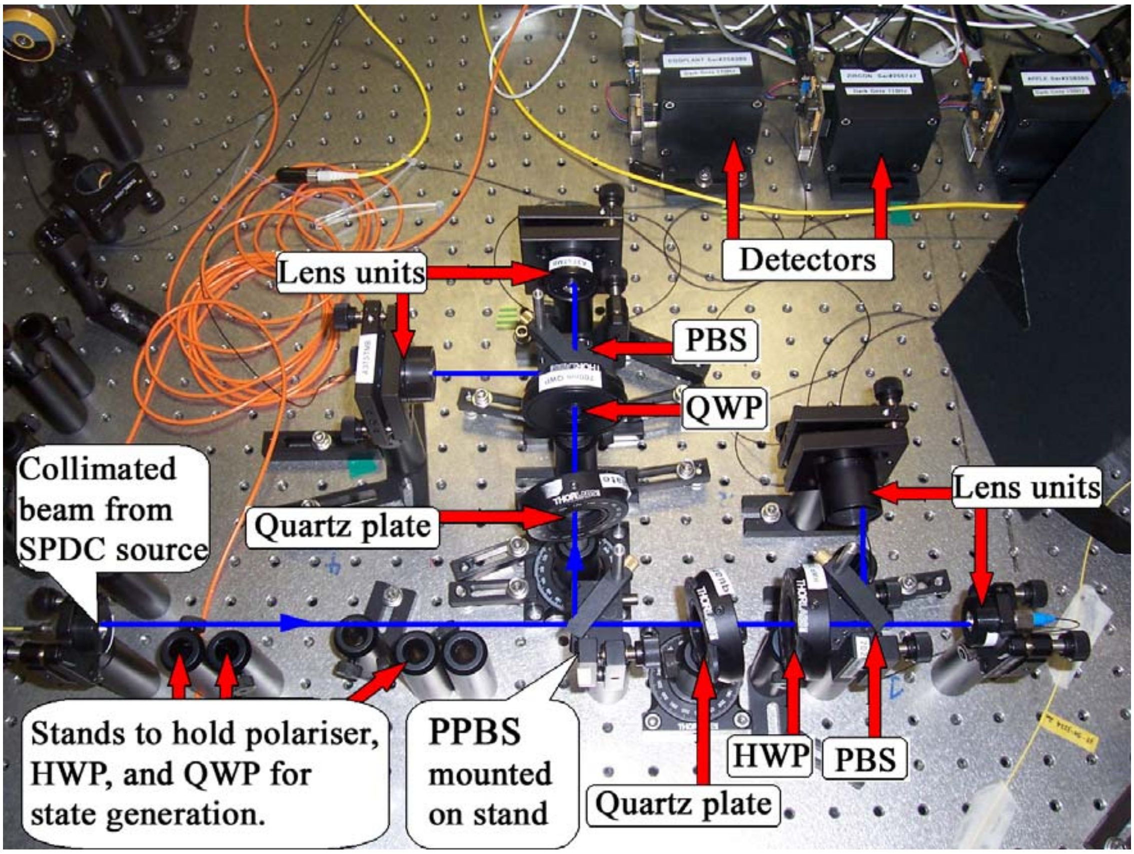

Figure A1: Picture of the experimental setup. Beam from the SPDC source is collimated and split into two paths by the partially polarising beam splitter (PPBS). Notice that the both the quartz plate are rotated slightly. The half-wave plate (HWP) in the transmitted arm is rotated to 22.5^{o}, while the quarter-wave plate (QWP) in the rotated arm is at 45^{o}. The lens units are connected to the detectors through optical fibres, and the detectors are in turn connected to the computer (not shown). Blue line represents the path of the light beam.

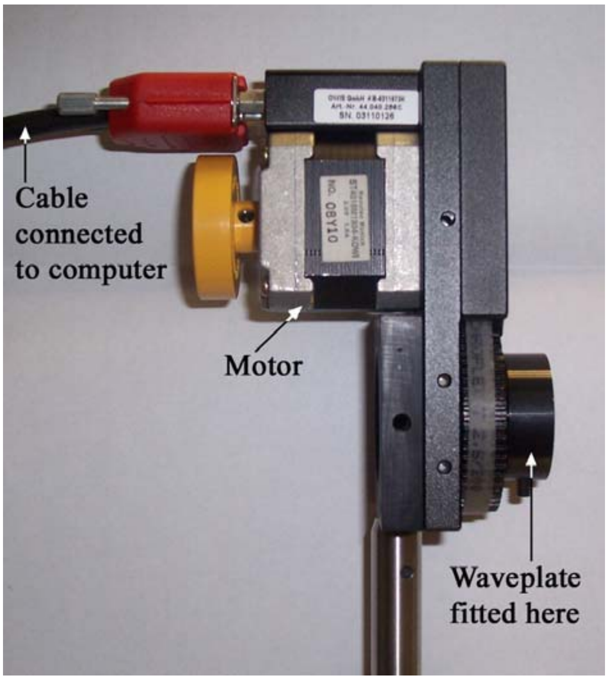

Figure A2: To generate the input states, the half-wave plate and quarter-wave plate are each fitted into the unit shown above and slotted into the empty holders before the PPBS (see previous figure). Rotation of the waveplates can then be controlled by the computer.

Bibliography

[1] J. Řeháček, B.-G. Englert, and D. Kaszlikowski, "Minimal qubit tomography," Phys. Rev. A **70**, 052321 (2004).

[2] D. F. V. James, P. G. Kwiat, W. J. Munro, and A. G. White, "Measurement of qubits," Phys. Rev. A **64**, 052312 (2001).

[3] B.-G. Englert *et al.*, "Highly Efficient Quantum Key Distribution with Minimal State Tomography," e-print arXiv: quant-ph/0412075 (2005).

[4] J. Anders, H. K. Ng, B.-G. Englert, and S. Y. Looi, "The Singapore Protocol: Incoherent Eavesdropping Attacks," e-print arXiv: quant-ph/0505069 (2005).

[5] E. Hecht, *Optics*, 4th ed. (Addison-Wesley, 2002), pp. 325-379.

[6] M. Born and E. Wolf, *Principles of Optics*, 6th (corr.) ed. (Cambridge University Press, Cambridge, United Kingdom, 1997), pp. 554.

[7] R. M. A. Azzam and N. M. Bashara, *Ellipsometry and Polarized Light* (North-Holland Pub. Co., New York, 1977), pp. 50.

[8] W. A. Shurcliff, *Polarized Light: Production and Use* (Harvard University Press, Cambridge, Mass., 1962), pp.168-169.

[9] J. B. Altepeter, E. R. Jeffrey, and P. G. Kwiat, "Photonic State Tomography," Notes on quantum state tomography by Kwiat Quantum Information Group, (http://www.physics.uiuc.edu/Research/QI/Photonics/Tomography/tomography_theory/ , 2005).

[10] M. G. Raymer and M. Beck, "Experimental Quantum State Tomography of Optical Fields and Ultrafast Statistical Sampling," in *Quantum State Estimation*, Lect. Notes Phys. **649**, edited by M. G. A. Paris and J. Řeháček (Springer, Berlin Heidelberg, 2004), pp. 243.

[11] H. E. Brandt, "Positive operator valued measure in quantum information processing," Am. J. Phys. **67** (5), 434-439 (1999).

[12] R. M. A. Azzam, "Arrangement of four photodetectors for measuring the state of polarization of light," Opt. Lett. **10** (7), 309-311 (1985).

[13] R. M. A. Azzam, I. M. Elminyawi, and A. M. El-Saba, "General analysis and optimization of the four-detector photopolarimeter," J. Opt. Soc. Am. A **5** (5), 681-689 (1988).

[14] A. Ambirajan and D. C. Look, "Optimum angles for a polarimeter: part I," Opt. Eng. **34** (6), 1651-1655 (1995).

[15] A. Ambirajan and D. C. Look, "Optimum angles for a polarimeter: part II," Opt. Eng. **34** (6), 1656-1658 (1995).

[16] R. M. A. Azzam, "Division-of-amplitude photopolarimeter (DOAP) for the simultaneous measure of all four Stokes parameters of light," Opt. Acta **29** (5), 685-689 (1982).

[17] R. M. A. Azzam. and A. De, "Optimal beam splitters for the division-of-amplitude photopolarimeter," J. Opt. Soc. Am. A **20** (5), 955-958 (2003).

[18] D. Poole, *Linear Algebra: a modern introduction* (Brooks/Cole, Pacific Grove, California, 2003), pp.272.

[19] I. Vaisman, *Analytical Geometry* (World Scientific, Singapore, 1997), pp. 37.

[20] B.-G. Englert, K. M. Tin, C. G. Goh, and H. K. Ng, "Single-loop interferometer for minimal ellipsometry," Laser Phys. **15**, 7-9 (2005).

[21] R. M. B. Clarke *et al.*, "Experimental realization of optimal detection strategies for overcomplete states," Phys. Rev. A **64**, 012303 (2001).

[22] R. M. A. Azzam and A. G. Lopez, "Accurate calibration of the four-detector photopolarimeter with imperfect polarizing optical elements," J. Opt. Soc. Am. A **6** (10), 1513-1521 (1989).

[23] R. Jozsa, "Fidelity for mixed quantum states," J. Mod. Opt. **41** (12), 2315-2323 (1994).

[24] W. Vogel and D.-G. Welsch, *Lectures on Quantum Optics* (Akademie Verlag, Berlin, 1994), pp. 253-264.